Computers & Security 157 (2025) 104533

Contents lists available at ScienceDirect

Computers & Security

journal homepage: www.elsevier.com/locate/cose

Full length article

New results on modeling and hybrid control for malware propagation in cyber–physical systems

Huifang Xiang, Ruimei Zhang *, Ziling Wang, Di Dong

School of Cyber Science and Engineering, Sichuan University, Chengdu Sichuan 610207, PR China

ARTICLE INFO

Keywords:
Cyber–physical systems
Malware propagation
Hopf bifurcation
Hybrid control

ABSTRACT

The structural characteristics of cyber–physical systems (CPSs) make them vulnerable to malware attacks. In order to study the propagation behavior of malware in CPSs, we propose a new malware propagation model, called Susceptible–Infected–Enhanced Infected–Quarantined–Recovered–Susceptible (SI2QRS) model. First, considering the feature that the infectiousness of malware may be enhanced during the propagation process, the SI2QRS model has two different infection rates. And the equilibrium points and the basic reproduction number of the model are derived. Second, the dynamic behavior is analyzed using stability theory and the bifurcation theorem. Given the bifurcation and chaos may arise in systems with time delay, a new hybrid controller is proposed to control the threshold of Hopf bifurcation. Finally, the simulation results show that the controller can bring the model to a stable state by delaying the threshold of Hopf bifurcation, which verifies the validity of the theoretical results.

1. Introduction

Driven by technologies such as big data, cloud computing, and the Internet of Things (IoT), the integration of the information space with the physical world is accelerating, leading to the emergence of cyber–physical systems (CPSs). CPSs, representing multidimensional complex systems, integrate computation, networking, and physical environments (Yu et al., 2023). Compared with classical embedded systems and network control systems (Oliveira et al., 2024), CPSs have the inherent characteristics of massive computation, real-time sensing, remote interaction, precise control and autonomous coordination, enabling flexible and efficient cross-domain monitoring, scientific decision-making and responsive actions in large-scale complex systems. Therefore, CPSs are widely used in key infrastructures such as smart grids, connected vehicles, intelligent healthcare, and industrial robots.

The development of electronic hardware in the field of computer systems has facilitated the continuous improvement of data processing capabilities and information transmission speed. As a result, industrial production has become highly reliant on CPSs characterized by digitization, networking and intelligence. However, the increasing openness of CPSs to various types and domains of network systems imposes higher requirements and makes CPSs more vulnerable to a wide range of network attacks. Common types of network attacks include Denial-of-Service (DoS) attacks (Ma et al., 2023), False Data Injection (FDI) attacks (Ma and Tsou, 2024), and replay attacks (Liu et al., 2021). Any occurrence of a network attack can result in various failures, rendering CPSs unable to function as intended and causing significant economic property loss. In 2016, the Mirai-infected botnets targeted popular websites, resulting in massive financial losses. The WannaCry ransomware virus in 2017 affected over 150 countries, causing billions of dollars in losses and disrupting critical industries. In April 2022, a ransomware attack in Costa Rica paralyzed government departments, leading to data theft and substantial financial losses. These cyber attacks highlight the severity of CPS security as an issue that cannot be ignored.

DoS attack is one of the main attacks against CPSs, and among the attack vectors of the DoS, malware emerges as one of the major threats (Wang et al., 2021). Given the similarities between malware propagation and infectious disease transmission in terms of environment (Carnier et al., 2024), propagation mechanisms (Gupta et al., 2022) and functionality (Li and Knickerbocker, 2007), Kephart and White (1992) first introduced the Susceptible–Infectious–Susceptible (SIS) model, integrating epidemiological methods (Bailey, 1975) with malware propagation. This model classifies nodes in a computer network into two states: infected (I) and susceptible (S). It is assumed that computers in the susceptible state may be infected by viruses, thereby transitioning into the infected state. By implementing various measures, such as installing antivirus

* Corresponding author.
E-mail address: ruimeizhang163@163.com (R. Zhang).

https://doi.org/10.1016/j.cose.2025.104533
Received 3 December 2024; Received in revised form 11 April 2025; Accepted 5 May 2025
Available online 3 June 2025

software (Kim et al., 2020) and regularly updating systems and software (Namanya et al., 2018), these computers are expected to revert to the susceptible state. Since then, many malware propagation models based on the fundamental biological virus model Susceptible–Infected–Recovered (SIR) model proposed by Kermack and McKendrick (1927) have been developed and improved to accommodate different types of malware scenarios. Considering that recovered computers may become susceptible again, the Susceptible–Infected–Recovered–Susceptible (SIRS) model was proposed (Zhang and Pan, 2021). However, malware typically requires a certain period to transition a susceptible computer into an infected state. Based on this consideration, Kharabsheh et al. (2024) introduced the Susceptible–Exposed–Infected–Recovered (SEIR) model, incorporating a new exposed (E) state. Subsequently, researchers have proposed various other malware propagation models based on different network characteristics, such as the Susceptible–Exposed–Infected–Recovered–Susceptible (SEIRS) model (Signes-Pont et al., 2018), the Susceptible–Exposed–Infected–Quarantined–Recovered (SEIQR) model (Lu and Lu, 2018), and the Susceptible–Exposed–Infected–Recovered–Susceptible with Vaccination and Quarantine (SEIQRV) model (Zarin et al., 2023). Biological infectious disease models and malware propagation models share several similarities but also have differences. In the biological virus models, factors like propagation rate and contact rate have clear biological meanings. In contrast, malware propagation models focus on dynamics within computer networks, where contact rates and infection rates are typically defined through non-biological factors, such as network topology. In recent biological infectious disease research, existing research has modeled the transmission of different strains of the same biological virus. For example, Abidemi et al. (2020) considered a dual-strain dengue fever coexistence model incorporating seasonal factors, demonstrating that seasonal variations significantly impact infection levels in human and vector populations. Kim et al. (2024) developed an SEIR model incorporating multiple COVID-19 variants and employed optimal control methods to analyze the effectiveness of different containment strategies. Additionally, in the context of avian influenza, Tadmon et al. (2024) established a dual-strain avian influenza model incorporating environmental transmission and viral mutation within the population. The propagation of malware in the digital environment is like the transmission of infection in a population, however, the spread of infection in the digital realm occurs at a significantly faster rate (Ginters et al., 2025). Given that the mutation characteristics of malware remain unexplored in existing CPSs security modeling research, we draw inspiration from biological virus transmission models. Incorporating malware propagation characteristics, a model is proposed with two distinct infection rates, which serves as the first motivation for our work.

When CPSs are attacked, malware may propagate between different computer network nodes and may lead to bifurcations in the CPSs, causing shocks and chaos. Therefore, there are many studies investigating the security of CPSs from the bifurcation control perspective. The commonly used methods include the state feedback method, delay feedback control method, parameter control method, and other control methods. Kumari and Upadhyay (2021) introduced a state feedback controller to the bifurcation problem of SIRS model to extend the stable region of the system and delay the occurrence of Hopf bifurcation in the network. Kiss et al. (2023) extended the control barrier function theory, which provides formal safety guarantees for delay-free systems, to systems with state delays, thereby presenting a theoretical framework for safety-critical control of time-delay systems. Dong and Zhao (2022) introduced an improved two-layer model considering time lag to describe the dynamic process of rumor propagation in multi-channel, and utilized particle swarm optimization algorithm to design an event-triggered pulse control strategy. Tian et al. (2023) proposed an effective strategy based on optimal dynamic immunization using a controlled dynamical model. For the hybrid control of CPSs, Yang et al. (2023) proposed three hybrid control strategies: continuous recovery, isolated delayed pulse isolation, and pulse charging. In order to prevent malware from propagating in CPSs, Zhang et al. (2022) presented an optimal control strategy by constructing a suitable Hamiltonian function. In CPSs, time delay is often considered as a kind of negative and unavoidable factor in signal transmission (Chen et al., 2023). Even though the disadvantage of time delay has been considered in previous works (Xu et al., 2021; Ghousein et al., 2023), most of the results tended to alleviate the adverse consequences caused by time delay, rather than using it to enhance the stability of the system. Therefore, how to design a hybrid control strategy that can utilize time delay to improve system stability is our second motivation.

Based on the above motivations, the contributions of this paper are as follows.

(i) A new model for malware propagation is proposed, which is called SI2QRS model. The model features two distinct infection rates and describes not only the malware propagation but also the potential enhancement of the malware infection rate during the propagation process.

(ii) A new hybrid control method is proposed, which integrates parameter adjustment and a memory feedback controller to utilize the time delay and improves system control efficiency. This hybrid control method is more flexible and provides better control by delaying the threshold of the Hopf bifurcation.

The subsequent sections of this paper are as follows. Section 2 introduces the SI2QRS malware propagation model. In Section 3, the stability of the malware propagation model at equilibrium points is analyzed. Section 4 analyzes the Hopf bifurcation of the model and presents a new hybrid control method. Section 5 validates the proposed model and methods through numerical simulations, and the real application based on Mirai's propagation is presented to show the effectiveness of the built SI2QRS model. Finally, Section 6 draws conclusions.

2. Modeling malware propagation in CPSs

When malicious software invades CPSs, it searches for nodes with software vulnerabilities and initiates attacks. Considering that the infectiousness of malware may be enhanced when it propagates in CPSs, we propose a new malicious software propagation model. To facilitate the subsequent model description, the symbol table is presented below, shown in Table 1.

We categorize all nodes in the system into five distinct types: susceptible nodes, infected nodes, enhanced infected nodes, quarantine nodes and recovery nodes. These five types are represented by the sets S, I_1, I_2, Q, and R respectively. Susceptible nodes, also known as vulnerable nodes, are easily targeted and exploited by malicious software. Nodes yet unaffected by malware fall into the susceptible category (S). When malware identifies vulnerable nodes and launches attack, susceptible nodes become infected nodes (I_1). As malware propagates within CPSs, it may update its components, enhancing its functionality and spreading capabilities. Consequently, susceptible nodes can transform into enhanced infected nodes (I_2). When nodes become infected, they may be discovered and subsequently quarantined by the system, which are denoted as quarantine nodes (Q). And the quarantine nodes will converse into recovery nodes (R). Then recovery nodes will lose their immunity to malware and transform back into susceptible nodes. Based on these considerations, we propose a new model called SI2QRS. At any given time t, the number of nodes in the categories S, I_1, I_2, Q, and R is represented as $S(t), I_1(t), I_2(t), Q(t)$ and $R(t)$ respectively. Additionally, the total number of nodes in CPSs is denoted as $N(t)$, and $N(t) = S(t) + I_1(t) + I_2(t) + Q(t) + R(t)$. The model is based on the following common assumptions (Yang et al., 2022):

(i) The system operates as a homogeneous field, allowing communication between any two nodes with equal probability.

(ii) The number of nodes of the system keeps a dynamic balance, and remains constant, i.e., the joining rate equals to the exiting rate, denoted as d. When the CPSs reach a stable operational state, the number of properly functioning nodes maintains a dynamic balance and remains constant, denoted as $N(t) = N$.

Table 1
Description of symbols of the SI2QRS system.

Symbol	Description
$S(t)$	The number of susceptible nodes at any given time t
$I_1(t)$	The number of infected nodes at any given time t
$I_2(t)$	The number of enhanced infected nodes at any given time t
$Q(t)$	The number of quarantine nodes at any given time t
$R(t)$	The number of recovered nodes at any given time t
α_1	Normal infection rate of susceptible nodes
α_2	Enhanced infection rate of susceptible nodes
β_1	Isolating rate from infected nodes to quarantine nodes
β_2	Isolating rate from enhanced infected nodes to quarantine nodes
a	Self-Recovery rate of infected nodes
b	Self-Recovery rate of enhanced infected nodes
r	Healing rate of quarantine nodes to recovery nodes
s	Transition rate of recovery nodes to susceptible nodes
d	Joining and exiting rate
R_0	The basic reproduction number of SI2QRS model

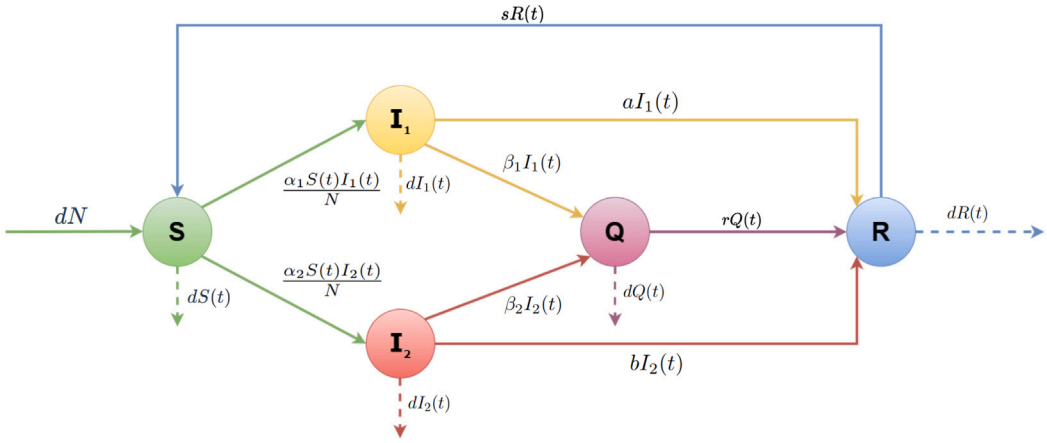

Fig. 1. Transition diagram between the different compartments of the model.

(iii) The infectious rate of I_1 is denoted as α_1, and the incidence law is given by $\frac{\alpha_1 S(t)I_1(t)}{N}$. The enhanced infectious rate of I_2 is represented by α_2, and the incidence law is expressed as $\frac{\alpha_2 S(t)I_1(t)}{N}$.

(iv) The parameters d, α_1, α_2, β_1, β_2, a, b, r, and s are all non-negative real constants.

Based on the above description, the transformation process of each node in the model is illustrated in Fig. 1. It is evident that S nodes can be infected at two distinct infectious rates, namely α_1 and α_2, resulting in the transformation into either infected nodes (I_1) or enhanced infected nodes (I_2). Infected nodes and enhanced infected nodes have the potential to be isolated and converted into quarantine nodes (Q) at rates of β_1 and β_2 respectively. Moreover, infected nodes and enhanced infected nodes can also be healed and transformed into recovery nodes (R) at rates of a and b respectively. Q nodes have the ability to transform into R nodes at the rate of r. Then R loses its immunity and turns back into a S node at the rate of s.

Based on the information provided in Fig. 1, the differential equations of the model are proposed as follows:

$$\begin{cases} \frac{dS(t)}{dt} = d(N - S(t)) - \frac{\alpha_1 S(t)I_1(t)}{N} - \frac{\alpha_2 S(t)I_2(t)}{N} + sR(t) \\ \frac{dI_1(t)}{dt} = \frac{\alpha_1 S(t)I_1(t)}{N} - \beta_1 I_1(t) - dI_1(t) - aI_1(t) \\ \frac{dI_2(t)}{dt} = \frac{\alpha_2 S(t)I_2(t)}{N} - \beta_2 I_2(t) - dI_2(t) - bI_2(t) \\ \frac{dQ(t)}{dt} = \beta_1 I_1(t) + \beta_2 I_2(t) - rQ(t) - dQ(t) \\ \frac{dR(t)}{dt} = rQ(t) + aI_1(t) + bI_2(t) - sR(t) - dR(t) \end{cases}, \tag{1}$$

where $S(t), I_1(t), I_2(t), Q(t), R(t) \geq 0$.

Dividing each equation by N in Eq. (1), the densities of each type of nodes in the total number are obtained, which are denoted as the differential equations of $\frac{S(t)}{N}, \frac{I_1(t)}{N}, \frac{I_2(t)}{N}, \frac{Q(t)}{N}, \frac{R(t)}{N}$. To simplify the expression of the model, let the distribution densities of each state nodes as new function variables, denoted as $\widetilde{S}(t), \widetilde{I}_1(t), \widetilde{I}_2(t), \widetilde{Q}(t)$ and $\widetilde{R}(t)$ respectively. Therefore, it can be obtained that the densities of nodes in five states should satisfy the normalization feature at any time ($t \geq 0$), i.e., $\widetilde{S}(t) + \widetilde{I}_1(t) + \widetilde{I}_2(t) + \widetilde{Q}(t) + \widetilde{R}(t) = 1$.

Due to the normalization condition, the system can be further expressed as follows:

$$\begin{cases} \frac{d\widetilde{I_1}(t)}{dt} = [\alpha_1(1-\widetilde{I}_1(t)-\widetilde{I}_2(t)-\widetilde{Q}(t)-\widetilde{R}(t))-\beta_1-d-a]\widetilde{I}_1(t) \\ \frac{d\widetilde{I_2}(t)}{dt} = [\alpha_2(1-\widetilde{I}_1(t)-\widetilde{I}_2(t)-\widetilde{Q}(t)-\widetilde{R}(t))-\beta_2-d-b]\widetilde{I}_2(t) \\ \frac{d\widetilde{Q}(t)}{dt} = \beta_1\widetilde{I}_1(t)+\beta_2\widetilde{I}_2(t)-r\widetilde{Q}(t)-d\widetilde{Q}(t) \\ \frac{d\widetilde{R}(t)}{dt} = r\widetilde{Q}(t)+a\widetilde{I}_1(t)+b\widetilde{I}_2(t)-s\widetilde{R}(t)-d\widetilde{R}(t) \end{cases}, \tag{2}$$

where $0 \le \widetilde{I}_1(t), \widetilde{I}_2(t), \widetilde{Q}(t), \widetilde{R}(t) \le 1, \quad 0 \le \widetilde{I}_1(t)+\widetilde{I}_2(t)+\widetilde{Q}(t)+\widetilde{R}(t) \le 1.$

In order to obtain the equilibrium points of SI2QRS model, letting $\frac{d\widetilde{I_1}(t)}{dt} = \frac{d\widetilde{I_2}(t)}{dt} = \frac{d\widetilde{Q}(t)}{dt} = \frac{d\widetilde{R}(t)}{dt} = 0$, we can identify three equilibrium points, which are represented as $E_0 = (0,0,0,0)$, $E_1 = (I_1^*, I_2^*, Q^*, R^*)$ and $E_2 = (I_{1e}, I_{2e}, Q_e, R_e)$, where

$$\begin{aligned} I_1^* &= \tfrac{(d+r)(d+s)(1-S^*)}{(d+r)(\alpha_1 S^*+s)+\beta_1 s}, & I_{1e} &= 0, \\ I_2^* &= 0, & I_{2e} &= \tfrac{(d+r)(d+s)(1-S_e)}{(d+r)(\alpha_2 S_e+s)+\beta_2 s}, \\ Q^* &= \tfrac{\beta_1(d+s)(1-S^*)}{(d+r)(\alpha_1 S^*+s)+\beta_1 s}, & Q_e &= \tfrac{\beta_2(d+s)(1-S_e)}{(d+r)(\alpha_2 S_e+s)+\beta_2 s}, \\ R^* &= \tfrac{(r\beta_1+a(r+d))(1-S^*)}{(d+r)(\alpha_1 S^*+s)+\beta_1 s}, & R_e &= \tfrac{(r\beta_2+b(r+d))(1-S_e)}{(d+r)(\alpha_2 S_e+s)+\beta_2 s}, \\ S^* &= \tfrac{a+\beta_1+d}{\alpha_1}, & S_e &= \tfrac{b+\beta_2+d}{\alpha_2}. \end{aligned}$$

In the field of epidemiology, the basic reproduction number R_0 is an important parameter for measuring the transmission capacity of an infectious disease. It quantifies the average number of individuals infected by an infectious individual in a completely susceptible population (Masood et al., 2019). A higher value of R_0 indicates a more challenging epidemic to control. To obtain the basic production number R_0, based on the next-generation matrix method (Van den Driessche and Watmough, 2002), let $X = (\widetilde{I}_1, \widetilde{I}_2, \widetilde{Q})^T$, then the following equation can be obtained

$$X = \begin{pmatrix} \widetilde{I}_1 \\ \widetilde{I}_2 \\ \widetilde{Q} \end{pmatrix} = F_{1,2}\left(\widetilde{I}_1, \widetilde{I}_2, \widetilde{Q}\right) - V_{1,2}\left(\widetilde{I}_1, \widetilde{I}_2, \widetilde{Q}\right), \tag{3}$$

where

$$F_{1,2}\left(\widetilde{I}_1, \widetilde{I}_2, \widetilde{Q}\right) = \begin{pmatrix} \alpha_1\widetilde{S}(t)\widetilde{I}_1(t) \\ \alpha_2\widetilde{S}(t)\widetilde{I}_2(t) \\ 0 \end{pmatrix}, V_{1,2}\left(\widetilde{I}_1, \widetilde{I}_2, \widetilde{Q}\right) = \begin{pmatrix} \left(\beta_1+d+a\right)\widetilde{I}_1(t) \\ \left(\beta_2+d+b\right)\widetilde{I}_2(t) \\ -\beta_1\widetilde{I}_1(t)-\beta_2\widetilde{I}_2(t)+d\widetilde{Q}(t)+r\widetilde{Q}(t) \end{pmatrix},$$

and the Jacobian matrices of $F_{1,2}$ and $V_{1,2}$ at E_0 can be obtained, denoted as F and V, where

$$F = Jacobian[F_{1,2}(\widetilde{I}_1, \widetilde{I}_2, \widetilde{Q})] = \begin{pmatrix} \alpha_1\widetilde{S}(0) & 0 & 0 \\ 0 & \alpha_2\widetilde{S}(0) & 0 \\ 0 & 0 & 0 \end{pmatrix},$$

$$V = Jacobian[V_{1,2}(\widetilde{I}_1, \widetilde{I}_2, \widetilde{Q})] = \begin{pmatrix} \beta_1+d+a & 0 & 0 \\ 0 & \beta_2+d+b & 0 \\ -\beta_1 & -\beta_2 & d+r \end{pmatrix}.$$

R_0 is computed as the spectral radius of the matrix FV^{-1}, which represents the maximum eigenvalue of the matrix. And its expression is as follows

$$R_0 = \rho(FV^{-1}) = \rho\begin{pmatrix} \frac{\alpha_1}{a+\beta_1+d}\widetilde{S}(0) & 0 & 0 \\ 0 & \frac{\alpha_2}{b+\beta_2+d}\widetilde{S}(0) & 0 \\ 0 & 0 & 0 \end{pmatrix}. \tag{4}$$

Due to $E_0 = (0,0,0,0)$ and $\widetilde{S}(t)+\widetilde{I}_1(t)+\widetilde{I}_2(t)+\widetilde{Q}(t)+\widetilde{R}(t) = 1$, it can be obtained that $\widetilde{S}(0) = 1$ at equilibrium E_0. Consequently, by substituting $\widetilde{S}(0) = 1$ in Eq. (4), it can be determined that $R_0 = \rho(FV^{-1}) = \max\{R_1, R_2\}$, where $R_1 = \frac{\alpha_1}{a+\beta_1+d}$ and $R_2 = \frac{\alpha_2}{b+\beta_2+d}$.

3. Stability analysis of equilibrium points in malware propagation model

Lemma 1 (*Lu and Lu, 2017*). *Let $f : D \in R^n \to R^n$ be a continuous and differentiable function. Considering an autonomous dynamic system $\dot{x} = f(x)$, we assume the following hypotheses:*

(H_1) *D is simply connected;*

(H_2) *There is a compact absorbing set $K \subset D$;*

(H_3) *The unique equilibrium x^* is in D.*

If there exist some positive numbers $\varepsilon_1, \varepsilon_2, \ldots, \varepsilon_n$ and $\tilde{B}(x)$, which is a matrix function, such that

$$\lim_{t\to+\infty}\sup_{x_0\in K}\frac{1}{t}\int_0^t\left[\tilde{b}_{ii}(s)+\sum_{i\neq j}\frac{\varepsilon_j}{\varepsilon_i}|\tilde{b}_{ij}(s)|\right]ds = \tilde{l}_i < 0, \tag{5}$$

then x^* is globally asymptotically stable, where $b_{ij}(t)$ represent entries of matrix $\tilde{B}(x)$ and $x(t, x_0)$ is the solution of the system when its initial value is x_0.

Define the state space of system (2) as Ω, where $\Omega = \{0 \le \widetilde{I}_1(t), \widetilde{I}_2(t), \widetilde{Q}(t), \widetilde{R}(t) \le 1, 0 \le \widetilde{I}_1(t) + \widetilde{I}_2(t) + \widetilde{Q}(t) + \widetilde{R}(t) \le 1\}$. Then the following results can be obtained.

Case 1. When $R_0 < 1$, $1 - S^* < 0$ and $1 - S_e < 0$, which means that $I_1^* = \frac{(d+r)(d+s)(1-S^*)}{(d+r)(\alpha_1 S^* + s) + \beta_1 s} < 0$ and $I_{2e} < 0$, as a result, $E_1 \notin \Omega$ and $E_2 \notin \Omega$. And it is obvious that $E_0 = (0, 0, 0, 0) \in \Omega$.

Case 2. When $R_0 > 1$ and $R_1 > R_2$, it can be obtained that $0 < I_1^* < 1$, $0 < Q^* < 1$, $0 < R^* < 1$, and $0 < I_1^* + I_2^* + Q^* + R^* < 1$, signifying that $E_1 \in \Omega$.

Case 3. When $R_0 > 1$ and $R_2 > R_1$, it can be obtained that $0 < I_{2e} < 1$, $0 < Q_e < 1$, $0 < R_e < 1$, and $0 < I_{1e} + I_{2e} + Q_e + R_e < 1$, signifying that $E_2 \in \Omega$.

Next, we will discuss the stability of the system (2) at the equilibrium points for each case.

For case 1, the system's stability at E_0 can be obtained, shown in Theorem 1.

Theorem 1. *When $R_0 < 1$, system (2) is locally and globally asymptotically stable at the disease-free equilibrium E_0.*

Proof. First, local stability is discussed. The Jacobian matrix of the system in Eq. (2) at E_0 is

$$J_{E_0} = \begin{bmatrix} \alpha_1 - \beta_1 - d - a & 0 & 0 & 0 \\ 0 & \alpha_2 - \beta_2 - d - b & 0 & 0 \\ \beta_1 & \beta_2 & -d - r & 0 \\ a & b & r & -d - s \end{bmatrix}.$$

The characteristic polynomial is

$$[\lambda - \alpha_1 + \beta_1 + d + a][\lambda - \alpha_2 + \beta_2 + d + b][\lambda + d + r][\lambda + d + s] = 0. \tag{6}$$

When $R_0 < 1$, the eigenvalues $\alpha_1 - \beta_1 - d - a, \alpha_2 - \beta_2 - d - b, -d - r$ and $-d - s$ in Eq. (6) are negative. Consequently, the model (2) is locally asymptotically stable at the disease-free equilibrium E_0.

To investigate the global asymptotically stability of system (2) at E_0, we choose a Lyapunov function as

$$V\left(\widetilde{I}_1, \widetilde{I}_2\right) = \frac{1}{2}\left(\widetilde{I}_1^{\,2} + \widetilde{I}_2^{\,2}\right).$$

It is clear that V is positive definite. Then, we take the derivative of V with respect to t:

$$\begin{aligned} \frac{dV}{dt} &= \widetilde{I}_1 \frac{d\widetilde{I}_1}{dt} + \widetilde{I}_2 \frac{d\widetilde{I}_2}{dt} \\ &= \widetilde{I}_1(t)^2 \left[\alpha_1 \left(1 - \widetilde{I}_1(t) - \widetilde{I}_2(t) - \widetilde{Q}(t) - \widetilde{R}(t)\right) - \beta_1 - d - a\right] \\ &+ \widetilde{I}_2(t)^2 \left[\alpha_2 \left(1 - \widetilde{I}_1(t) - \widetilde{I}_2(t) - \widetilde{Q}(t) - \widetilde{R}(t)\right) - \beta_2 - d - b\right] \\ &\le (\alpha_1 - \beta_1 - d - a)\widetilde{I}_1(t)^2 + (\alpha_2 - \beta_2 - d - b)\widetilde{I}_2(t)^2 \le 0. \end{aligned}$$

$\frac{dV}{dt} = 0$ if and only if $\widetilde{I}_1 = 0, \widetilde{I}_2 = 0$ and $V \to \infty (\widetilde{I}_1 \to \infty$ and $\widetilde{I}_2 \to \infty)$. By the Lyapunov's stability theorem, system (2) is global asymptotically stable at E_0. It completes the proof.

For case 2, the following theorem can be obtained.

Theorem 2. *When $R_0 > 1$ and $R_1 > R_2$, system (2) is locally asymptotically stable at E_1. Moreover, when*

$$r + s + 2d > max\{a + \beta_1, b + \beta_2\}, \tag{7}$$

model (2) is globally asymptotically stable at E_1.

Proof. To investigate the local stability, taking E_1 into consideration, the Jacobian matrix of the system at E_1 is

$$J_{E_1} = \begin{bmatrix} -\alpha_1 I_1^* & -\alpha_1 I_1^* & -\alpha_1 I_1^* & -\alpha_1 I_1^* \\ 0 & \alpha_2 S^* - \beta_2 - d - b & 0 & 0 \\ \beta_1 & \beta_2 & -d - r & 0 \\ a & b & r & -d - s \end{bmatrix}.$$

The characteristic polynomial of J_{E_1} is $\lambda^4 + a_1\lambda^3 + a_2\lambda^2 + a_3\lambda + a_4 = 0$, where

$$a_1 = q_1 + q_2, \quad a_2 = q_1 q_2 + q_3, \quad a_3 = q_1 q_3 + q_4, \quad a_4 = q_1 q_4,$$

and

$$\begin{aligned} q_1 &= b + \beta_2 + d - S^*\alpha_2, q_3 = dr + ds + rs + d^2 + I_1^* a\alpha_1 + I_1^*\alpha_1\beta_1 + 2I_1^*\alpha_1 d + I_1^*\alpha_1 r + I_1^*\alpha_1 s, \\ q_2 &= 2d + r + s + I_1^*\alpha_1, q_4 = I_1^*\alpha_1 d^2 + I_1^* a\alpha_1 d + I_1^*\alpha_1\beta_1 d + I_1^* a\alpha_1 r + I_1^*\alpha_1\beta_1 r + I_1^*\alpha_1\beta_1 s + I_1^*\alpha_1 dr + I_1^*\alpha_1 ds + I_1^*\alpha_1 rs. \end{aligned}$$

Then, we obtain

$$\begin{aligned} &\Delta_1 = a_1 = q_1 + q_2, \\ &\Delta_2 = a_1 a_2 - a_3 = (q_1 + q_2)(q_1 q_2 + q_3) - q_1 q_3 - q_4, \\ &\Delta_3 = a_1\left(a_2 a_3 - a_1 a_4\right) - a_3^2. \end{aligned}$$

By simple calculation, we can prove that $\Delta_1 > 0$, $\Delta_2 > 0$ and $\Delta_3 > 0$ (the full proof is provided in Appendix A). According to the Routh–Hurwitz criterion, the model (2) is locally asymptotically stable at E_1.

Then we discuss the global stability of E_1. Define $K(x) = \widetilde{S} + \widetilde{I}_1 + \widetilde{I}_2 + \widetilde{Q} + \widetilde{R} - 1$ with $x = (\widetilde{S}, \widetilde{I}_1, \widetilde{I}_2, \widetilde{Q}, \widetilde{R}) \in R_+^5$. Obviously, system (2) admits an invariant manifold $D = \{x \in R_+^5 | K(x) = 0\}$. System (2) is locally stable at E_1, which implies the existence of a constant $e_0 > 0$ such that:

$$e_0 \le \widetilde{S}, \widetilde{I}_1, \widetilde{I}_2, \widetilde{Q}, \widetilde{R} \le 1. \tag{8}$$

And there exists a compact set $K \subset D$ which absorbs any solutions of model (2).

Let the Jacobian matrix of Eq. (2) be J. Then we can obtain

$$J = \begin{bmatrix} W - (\beta_1 + d + a) & -\alpha_1 \widetilde{I}_1 & -\alpha_1 \widetilde{I}_1 & -\alpha_1 \widetilde{I}_1 \\ -\alpha_2 \widetilde{I}_2 & Z - (\beta_2 + d + b) & -\alpha_2 \widetilde{I}_2 & -\alpha_2 \widetilde{I}_2 \\ \beta_1 & \beta_2 & -r - d & 0 \\ a & b & r & -s - d \end{bmatrix} \triangleq \begin{bmatrix} J_{11} & J_{12} & J_{13} & J_{14} \\ J_{21} & J_{22} & J_{23} & J_{24} \\ J_{31} & J_{32} & J_{33} & J_{34} \\ J_{41} & J_{42} & J_{43} & J_{44} \end{bmatrix},$$

where $W = \alpha_1(1 - 2\widetilde{I}_1 - \widetilde{I}_2 - \widetilde{Q} - \widetilde{R})$, $Z = \alpha_2(1 - \widetilde{I}_1 - 2\widetilde{I}_2 - \widetilde{Q} - \widetilde{R})$. According to Li and Muldowney (2000), the third additive matrix of J, denoted as J^3, is as follows:

$$J^3 = \begin{bmatrix} J_{11} + J_{22} + J_{33} & J_{34} & -J_{24} & J_{14} \\ J_{43} & J_{11} + J_{22} + J_{44} & J_{23} & -J_{13} \\ -J_{42} & J_{32} & J_{11} + J_{33} + J_{44} & J_{12} \\ J_{41} & -J_{31} & J_{21} & J_{22} + J_{33} + J_{44} \end{bmatrix}$$

$$= \begin{bmatrix} J_{11} + J_{22} + J_{33} & 0 & \alpha_2 I_2 & -\alpha_1 I_1 \\ r & J_{11} + J_{22} + J_{44} & -\alpha_2 I_2 & \alpha_1 I_1 \\ -b & \beta_2 & J_{11} + J_{33} + J_{44} & -\alpha_1 I_1 \\ a & -\beta_1 & -\alpha_2 I_2 & J_{22} + J_{33} + J_{44} \end{bmatrix},$$

where

$$J_{11} + J_{22} + J_{33} = W + Z - (\beta_1 + 3d + a + \beta_2 + b + r), \quad J_{11} + J_{33} + J_{44} = W - (\beta_1 + 3d + a + r + s),$$
$$J_{11} + J_{22} + J_{44} = W + Z - (\beta_1 + 3d + a + \beta_2 + b + s), \quad J_{22} + J_{33} + J_{44} = Z - (\beta_2 + 3d + b + r + s).$$

Let $\dot{\widetilde{I}}_1 = \frac{d\widetilde{I}_1(t)}{dt}$ and $\dot{\widetilde{I}}_2 = \frac{d\widetilde{I}_2(t)}{dt}$, set $H = diag\{\frac{\widetilde{I}_1}{\widetilde{I}_2}, \frac{\widetilde{I}_1}{\widetilde{I}_2}, \frac{\widetilde{I}_1}{\widetilde{I}_2}, \frac{\widetilde{I}_1}{\widetilde{I}_2}\}$, denoting the derivation of H as H_f, we have $H_f = diag\{\frac{\dot{\widetilde{I}}_1}{\widetilde{I}_1} - \frac{\widetilde{I}_1\dot{\widetilde{I}}_2}{\widetilde{I}_2^2}, \frac{\dot{\widetilde{I}}_1}{\widetilde{I}_1} - \frac{\widetilde{I}_1\dot{\widetilde{I}}_2}{\widetilde{I}_2^2}, \frac{\dot{\widetilde{I}}_1}{\widetilde{I}_1} - \frac{\widetilde{I}_1\dot{\widetilde{I}}_2}{\widetilde{I}_2^2}, \frac{\dot{\widetilde{I}}_1}{\widetilde{I}_1} - \frac{\widetilde{I}_1\dot{\widetilde{I}}_2}{\widetilde{I}_2^2}\}$, then $H_f H^{-1} = diag\{\frac{\dot{\widetilde{I}}_1}{\widetilde{I}_1} - \frac{\dot{\widetilde{I}}_2}{\widetilde{I}_2}, \frac{\dot{\widetilde{I}}_1}{\widetilde{I}_1} - \frac{\dot{\widetilde{I}}_2}{\widetilde{I}_2}, \frac{\dot{\widetilde{I}}_1}{\widetilde{I}_1} - \frac{\dot{\widetilde{I}}_2}{\widetilde{I}_2}, \frac{\dot{\widetilde{I}}_1}{\widetilde{I}_1} - \frac{\dot{\widetilde{I}}_2}{\widetilde{I}_2}\}$. Let

$$B = H_f H^{-1} + H J^3 H^{-1},$$

then $B =$

$$\begin{bmatrix} J_{11} + J_{22} + J_{33} + \frac{\dot{I}_1}{I_1} - \frac{\dot{I}_2}{I_2} & 0 & \alpha_2 I_2 & -\alpha_1 I_1 \\ r & J_{11} + J_{22} + J_{44} + \frac{\dot{I}_1}{I_1} - \frac{\dot{I}_2}{I_2} & -\alpha_2 I_2 & \alpha_1 I_1 \\ -b & \beta_2 & J_{11} + J_{33} + J_{44} + \frac{\dot{I}_1}{I_1} - \frac{\dot{I}_2}{I_2} & -\alpha_1 I_1 \\ a & -\beta_1 & -\alpha_2 I_2 & J_{22} + J_{33} + J_{44} + \frac{\dot{I}_1}{I_1} - \frac{\dot{I}_2}{I_2} \end{bmatrix}.$$

In addition, the system (2) can be rewritten as

$$\begin{cases} \frac{\dot{\widetilde{I}}_1}{\widetilde{I}_1} + \beta_1 + d + a = \alpha_1(1 - \widetilde{I}_1(t) - \widetilde{I}_2(t) - \widetilde{Q}(t) - \widetilde{R}(t)), \\ \frac{\dot{\widetilde{I}}_2}{\widetilde{I}_2} + \beta_2 + d + b = \alpha_2(1 - \widetilde{I}_1(t) - \widetilde{I}_2(t) - \widetilde{Q}(t) - \widetilde{R}(t)), \\ \frac{\dot{\widetilde{Q}}}{\widetilde{Q}} + r + d = \frac{\beta_1 \widetilde{I}_1(t) + \beta_2 \widetilde{I}_2(t)}{\widetilde{Q}}, \\ \frac{\dot{\widetilde{R}}}{\widetilde{R}} + s + d = \frac{r\widetilde{Q}(t) + a\widetilde{I}_1(t) + b\widetilde{I}_2(t)}{\widetilde{R}}. \end{cases}$$

Let b_{ij} represent entries of matrix B, consequently,

$$\begin{aligned} h_1(t) &= b_{11} + \sum_{j=2}^{4} \left|b_{1j}\right| \\ &= J_{11} + J_{22} + J_{33} + \frac{\dot{\widetilde{I}}_1}{\widetilde{I}_1} - \frac{\dot{\widetilde{I}}_2}{\widetilde{I}_2} + \alpha_2 \widetilde{I}_2 + \alpha_1 \widetilde{I}_1 \\ &= \alpha_1(1 - 2\widetilde{I}_1 - \widetilde{I}_2 - \widetilde{Q} - \widetilde{R}) + \alpha_2(1 - \widetilde{I}_1 - 2\widetilde{I}_2 - \widetilde{Q} - \widetilde{R}) - (\beta_1 + 3d + a + \beta_2 + b + r) + \frac{\dot{\widetilde{I}}_1}{\widetilde{I}_1} - \frac{\dot{\widetilde{I}}_2}{\widetilde{I}_2} \\ &+ \alpha_2 \widetilde{I}_2 + \alpha_1 \widetilde{I}_1 \le -r + 2\frac{\dot{\widetilde{I}}_1}{\widetilde{I}_1}. \end{aligned}$$

Similarly,

$$h_2(t) = b_{22} + \sum_{j \ne 2} \left|b_{2j}\right| = J_{11} + J_{22} + J_{44} + \frac{\dot{\widetilde{I}}_1}{\widetilde{I}_1} - \frac{\dot{\widetilde{I}}_2}{\widetilde{I}_2} + \alpha_2 \widetilde{I}_2 + \alpha_1 \widetilde{I}_1 \le -s - d + 2\frac{\dot{\widetilde{I}}_2}{\widetilde{I}_2},$$
$$h_3(t) = b_{33} + \sum_{j \ne 3} \left|b_{3j}\right| = J_{11} + J_{33} + J_{44} + \frac{\dot{\widetilde{I}}_1}{\widetilde{I}_1} - \frac{\dot{\widetilde{I}}_2}{\widetilde{I}_2} + \alpha_1 \widetilde{I}_1 + b + \beta_2 \le -2d - r - s + b + \beta_2 + 2\frac{\dot{\widetilde{I}}_1}{\widetilde{I}_1},$$
$$h_4(t) = b_{44} + \sum_{j \ne 3} \left|b_{1j}\right| = J_{22} + J_{33} + J_{44} + \frac{\dot{\widetilde{I}}_1}{\widetilde{I}_1} - \frac{\dot{\widetilde{I}}_2}{\widetilde{I}_2} + \alpha_2 \widetilde{I}_2 + a + \beta_1 \le -2d - r - s + a + \beta_1 + \frac{\dot{\widetilde{I}}_1}{\widetilde{I}_1}.$$

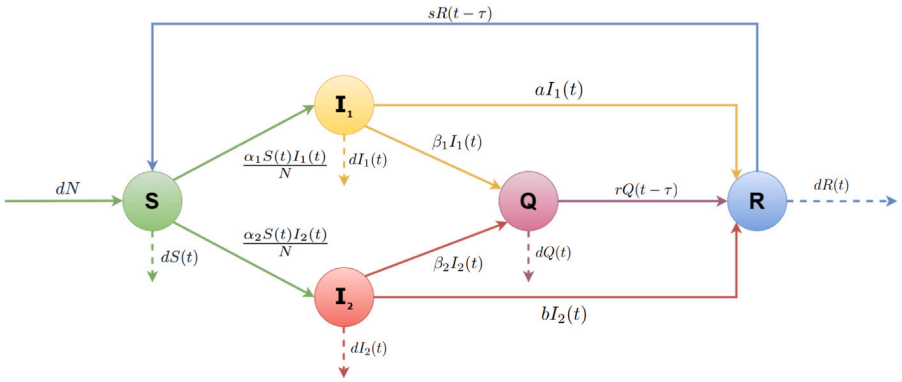

Fig. 2. Transition diagram between the different compartments of the model with time delay.

Set

$$-r+2\frac{\widetilde{I_1}}{\widetilde{I_1}} \triangleq \bar{h}_1(t), \quad -s-d+2\frac{\widetilde{I_2}}{\widetilde{I_2}} \triangleq \bar{h}_2(t),$$
$$-2d-r-s+b+\beta_2+2\frac{\widetilde{I_1}}{\widetilde{I_1}} \triangleq \bar{h}_3(t), \quad -2d-r-s+a+\beta_1+\frac{\widetilde{I_1}}{\widetilde{I_1}} \triangleq \bar{h}_4(t).$$

Let the matrix $C(t)$ be $C(t) = \text{diag}\left\{\bar{h}_1(t), \bar{h}_2(t), \bar{h}_3(t), \bar{h}_4(t)\right\}$. Based on Eq. (8), we get

$$\lim_{t\to+\infty} \frac{1}{t}\int_0^t \bar{h}_i(t)dt = \bar{h}_i,$$

where

$$\bar{h}_1 = -r, \quad \bar{h}_2 = -s-d, \quad \bar{h}_3 = -2d-r-s+b+\beta_2, \quad \bar{h}_4 = -2d-r-s+a+\beta_1.$$

According to the condition (7), it can be easily obtained that $\bar{h}_1, \bar{h}_2, \bar{h}_3, \bar{h}_4 < 0$. According to Lemma 1, the system is globally asymptotically stable at E_1.

Remark 1. Lemma 1 is based on the geometric criterion. It provides a general criterion for the global asymptotic stability of equilibrium points in nonlinear autonomous differential equations without requiring the explicit construction of a Lyapunov function. In this case, when the system satisfies the conditions in Eq. (5), i.e., Theorem 2.6 from Lu and Lu (2017), it reaches the result in Theorem 2.

For case 3, we have the following result, shown in Theorem 3.

Theorem 3. *When $R_0 > 1$ and $R_2 > R_1$, system (2) is locally asymptotically stable at E_2.*

Proof. The full proof is provided in Appendix B.

4. Bifurcation and control analysis of malware propagation model with time delay

Considering the malware propagation characteristics in real-world CPSs, time delays are unavoidable (Chen et al., 2023). In the model (2), Q nodes turn to R nodes after a period of isolation, and R nodes lose immunity and revert to S nodes after a certain period. Thus, we design a delayed SI2QRS model, introducing time delay τ into these node transition processes, as shown in Fig. 2.

Due to the normalization condition, the differential equations of delayed SI2QRS model are derived as follows:

$$\begin{cases} \frac{d\widetilde{I_1}(t)}{dt} = [\alpha_1(1-\widetilde{I_1}(t)-\widetilde{I_2}(t)-\widetilde{Q}(t)-\widetilde{R}(t))-\beta_1-d-a]\widetilde{I_1}(t) \\ \frac{d\widetilde{I_2}(t)}{dt} = [\alpha_2(1-\widetilde{I_1}(t)-\widetilde{I_2}(t)-\widetilde{Q}(t)-\widetilde{R}(t))-\beta_2-d-b]\widetilde{I_2}(t) \\ \frac{d\widetilde{Q}(t)}{dt} = \beta_1\widetilde{I_1}(t)+\beta_2\widetilde{I_2}(t)-r\widetilde{Q}(t-\tau)-d\widetilde{Q}(t) \\ \frac{d\widetilde{R}(t)}{dt} = r\widetilde{Q}(t-\tau)+a\widetilde{I_1}(t)+b\widetilde{I_2}(t)-s\widetilde{R}(t-\tau)-d\widetilde{R}(t) \end{cases}. \tag{9}$$

However, the presence of time delays in a model system can render a stable equilibrium unstable, leading to bifurcations and chaos (Barman and Mishra, 2024). Therefore, we analyze the conditions under which bifurcation occurs in this model (9) and propose a corresponding control method.

4.1. Bifurcation analysis of malware propagation model

In this section, we determine sufficient and necessary conditions for Hopf bifurcation to occur using the time delay τ as the bifurcation parameter.

When assuming $R_0 = R_1 > R_2$, we consider the effect of the time delay τ on the local stability of E_1. Using the time delay τ as the bifurcation parameter, the characteristic polynomial at E_1 of the system in Eq. (9) is

$$0 = \det\begin{bmatrix} \lambda+\alpha_1 I_1^* & \alpha_1 I_1^* & \alpha_1 I_1^* & \alpha_1 I_1^* \\ 0 & \lambda+\beta_2+d+b-\alpha_2 S^* & 0 & 0 \\ -\beta_1 & -\beta_2 & \lambda+d+re^{-\lambda\tau} & 0 \\ -a & -b & -re^{-\lambda\tau} & \lambda+d+se^{-\lambda\tau} \end{bmatrix}, \tag{10}$$

leading to the equation:

$$\lambda^4 + c_1\lambda^3 + c_2\lambda^2 + c_3\lambda + c_4 + (c_5\lambda^3 + c_6\lambda^2 + c_7\lambda + c_8)e^{-\lambda\tau} + (c_9\lambda^2 + c_{10}\lambda + c_{11})e^{-2\lambda\tau} = 0, \tag{11}$$

where

$$\begin{aligned}
c_1 &= b+\beta_2+3d+I_1^*\alpha_1 - S^*\alpha_2,\\
c_2 &= 2bd+2\beta_2 d+3d^2+I_1^*a\alpha_1+I_1^*\alpha_1 b+I_1^*\alpha_1\beta_1+I_1^*\alpha_1\beta_2+3I_1^*\alpha_1 d-2S^*\alpha_2 d-I_1^*S^*\alpha_1\alpha_2,\\
c_3 &= bd^2+\beta_2 d^2+d^3+3I_1^*\alpha_1 d^2-S^*\alpha_2 d^2+I_1^*a\alpha_1 b+I_1^*a\alpha_1\beta_2+I_1^*\alpha_1 b\beta_1+I_1^*\alpha_1\beta_1\beta_2+2I_1^*a\alpha_1 d+2I_1^*\alpha_1 bd\\
&\quad +2I_1^*\alpha_1\beta_1 d+2I_1^*\alpha_1\beta_2 d-I_1^*S^*a\alpha_1\alpha_2-I_1^*S^*\alpha_1\alpha_2\beta_1-2I_1^*S^*\alpha_1\alpha_2 d,\\
c_4 &= I_1^*\alpha_1 d^3+I_1^*a\alpha_1 d^2+I_1^*\alpha_1 bd^2+I_1^*\alpha_1\beta_1 d^2+I_1^*\alpha_1\beta_2 d^2+I_1^*a\alpha_1 bd+I_1^*a\alpha_1\beta_2 d+I_1^*\alpha_1 b\beta_1 d+I_1^*\alpha_1\beta_1\beta_2 d\\
&\quad -I_1^*S^*\alpha_1\alpha_2 d^2-I_1^*S^*a\alpha_1\alpha_2 d-I_1^*S^*\alpha_1\alpha_2\beta_1 d, \quad c_5 = r+s,\\
c_6 &= br+\beta_2 r+bs+\beta_2 s+2dr+2ds+I_1^*\alpha_1 r+I_1^*\alpha_1 s-S^*\alpha_2 r-S^*\alpha_2 s,\\
c_7 &= d^2 r+d^2 s+bdr+\beta_2 dr+bds+\beta_2 ds+I_1^*a\alpha_1 r+I_1^*\alpha_1 br+I_1^*\alpha_1\beta_1 r+I_1^*\alpha_1\beta_2 r+I_1^*\alpha_1 bs+I_1^*\alpha_1\beta_1 s\\
&\quad +I_1^*\alpha_1\beta_2 s+2I_1^*\alpha_1 dr+2I_1^*\alpha_1 ds-S^*\alpha_2 dr-S^*\alpha_2 ds-I_1^*S^*\alpha_1\alpha_2 r-I_1^*S^*\alpha_1\alpha_2 s,\\
c_8 &= I_1^*\alpha_1 d^2 r+I_1^*\alpha_1 d^2 s+I_1^*a\alpha_1 br+I_1^*a\alpha_1\beta_2 r+I_1^*\alpha_1 b\beta_1 r+I_1^*\alpha_1\beta_1\beta_2 r+I_1^*a\alpha_1 dr+I_1^*\alpha_1 b\beta_1 s+I_1^*\alpha_1\beta_1\beta_2 s\\
&\quad +I_1^*\alpha_1 bdr+I_1^*\alpha_1\beta_1 dr+I_1^*\alpha_1\beta_2 dr+I_1^*\alpha_1 bds+I_1^*\alpha_1\beta_1 ds+I_1^*\alpha_1\beta_2 ds-I_1^*S^*a\alpha_1\alpha_2 r-I_1^*S^*\alpha_1\alpha_2\beta_1 r\\
&\quad -I_1^*S^*\alpha_1\alpha_2\beta_1 s-I_1^*S^*\alpha_1\alpha_2 dr-I_1^*S^*\alpha_1\alpha_2 ds, \quad c_9 = rs,\\
c_{10} &= brs+\beta_2 rs+drs+I_1^*\alpha_1 rs-S^*\alpha_2 rs, \quad c_{11} = I_1^*\alpha_1 brs+I_1^*\alpha_1\beta_2 rs+I_1^*\alpha_1 drs-I_1^*S^*\alpha_1\alpha_2 rs.
\end{aligned}$$

Multiplying the two sides of Eq. (11) by $e^{\lambda\tau}$, we obtain

$$(\lambda^4 + c_1\lambda^3 + c_2\lambda^2 + c_3\lambda + c_4)e^{\lambda\tau} + (c_5\lambda^3 + c_6\lambda^2 + c_7\lambda + c_8) + (c_9\lambda^2 + c_{10}\lambda + c_{11})e^{-\lambda\tau} = 0. \tag{12}$$

Let Eq. (11) have a pure imaginary root $\lambda = i\omega$ where i is the imaginary unit, and substitute it into Eq. (12), then the following formula can be obtained

$$\begin{cases} (w^4 - c_2w^2 - c_9w^2 + c_{11})\cos(w\tau) + (c_1w^3 - c_3w + c_{10}w)\sin(w\tau) = c_6w^2 - c_8 \\ (-c_1w^3 + c_3w + c_{10}w)\cos(w\tau) + (w^4 - c_2w^2 + c_9w^2 - c_{11})\sin(w\tau) = c_5w^3 - c_7w. \end{cases} \tag{13}$$

Let

$$\begin{aligned}
&d_1 = c_6 - c_1c_5, \quad d_2 = -c_8 + c_1c_7 - c_2c_6 + c_3c_5 - c_5c_{10} + c_6c_9,\\
&d_3 = c_2c_8 - c_3c_7 - c_6c_{11} + c_7c_{10} - c_8c_9, \quad d_4 = c_8c_{11}, \quad d_5 = c_5,\\
&d_6 = -c_7 + c_1c_6 - c_2c_5 - c_5c_9, \quad d_7 = -c_1c_8 + c_2c_7 - c_3c_6 + c_5c_{11} - c_6c_{10} + c_7c_9,\\
&d_8 = c_3c_8 - c_7c_{11} + c_8c_{10}, \quad d_9 = -2c_2 + c_1^2, \quad d_{10} = c_2^2 - c_9^2 - 2c_1c_3,\\
&d_{11} = -c_{10}^2 + c_3^2 + 2c_9c_{11}, \quad d_{12} = -c_{11}^2,
\end{aligned}$$

then $\cos w\tau$ and $\sin w\tau$ can be written as

$$\begin{cases} \cos(w\tau) = \frac{d_1w^6+d_2w^4+d_3w^2+d_4}{w^8+d_9w^6+d_{10}w^4+d_{11}w^2+d_{12}} \\ \sin(w\tau) = \frac{d_5w^7+d_6w^5+d_7w^3+d_8w}{w^8+d_9w^6+d_{10}w^4+d_{11}w^2+d_{12}} \end{cases}. \tag{14}$$

The sum of the squares of the two formulas in Eq. (14) is obtained

$$f(w) = w^{16} + m_1w^{14} + m_2w^{12} + m_3w^{10} + m_4w^8 + m_5w^6 + m_6w^4 + m_7w^2 + m_8 = 0, \tag{15}$$

where

$$\begin{aligned}
&m_1 = -d_5^2 + 2d_9, m_2 = -d_1^2 + d_9^2 + 2d_{10} - 2d_5d_6,\\
&m_3 = -d_6^2 + 2d_{11} - 2d_1d_2 - 2d_5d_7 + 2d_9d_{10},\\
&m_4 = -d_2^2 + d_{10}^2 + 2d_{12} - 2d_1d_3 - 2d_5d_8 - 2d_6d_7 + 2d_9d_{11},\\
&m_5 = -d_7^2 - 2d_1d_4 - 2d_2d_3 - 2d_6d_8 + 2d_9d_{12} + 2d_{10}d_{11},\\
&m_6 = -d_3^2 + d_{11}^2 - 2d_2d_4 - 2d_7d_8 + 2d_{10}d_{12}, m_7 = -d_8^2 - 2d_3d_4 + 2d_{11}d_{12}, m_8 = -d_4^2 + d_{12}^2.
\end{aligned}$$

Proposition 1. *If $m_8 < 0$, Eq. (15) has at least one positive real root, with the count of such roots not exceeding eight.*

Proof. Since $\lim_{x\to\infty} f(x) = +\infty$, we conclude that Eq. (15) has at least a positive real root if $f(0) = m_8 < 0$. And the number of the positive real roots is not greater than 8 due to $f(w_0)$ being a 16-order even polynomial. Suppose Eq. (15) has $n(n \le 8)$ positive real roots $\omega_k, k = 1, \dots, n$. By Eq. (14), we have

$$\tau_k^{(j)} = \frac{1}{w_k}\left(\arccos\frac{d_1w_k^6 + d_2w_k^4 + d_3w_k^2 + d_4}{w_k^8 + d_9w_k^6 + d_{10}w_k^4 + d_{11}w_k^2 + d_{12}} + 2j\pi\right), \text{ where } k = 1, \dots, n; j = 0, 1, 2, \dots.$$

And we choose $\tau_0 = \min_{k,j} \tau_k^{(j)}$. When $\tau = \tau_0$, the Jacobian matrix of the system matrix E_1 possesses a pair of conjugate complex eigenvalues $\pm i\omega_0$. In this case, the corresponding ω_0 is a positive real root of Eq. (15).

Theorem 4. *When $R_0 > 1$, $R_1 > R_2$ and $m_8 < 0$, then the system in Eq. (9) is locally asymptotically stable at E_1 for any $\tau \in [0, \tau_0)$.*

Proof. According to Theorem 2, the system (9) is locally asymptotically stable at E_1 when $\tau = 0$. Combining THEOREM 6.1 in Freedman and Hari Rao (1983), it follows that E_1 is locally asymptotically stable when $0 \le \tau < \tau_0$.

Theorem 5. *When $R_0 > 1$, $R_1 > R_2, m_8 < 0$ and $\tau = \tau_0$, system (9) undergoes a Hopf bifurcation at E_1 if $n_1 n_3 + n_2 n_4 \neq 0$, where*

$$\begin{cases} n_1 = \left(-3c_1\omega_0^2 + c_3 + c_{10}\right)\cos(\omega_0\tau_0) + \left(4\omega_0^3 - 2c_2\omega_0 + 2c_9\omega_0\right)\sin(\omega_0\tau_0) - 3c_5\omega_0^2 + c_7 \\ n_2 = \left(-4\omega_0^3 + 2c_2\omega_0 + 2c_9\omega_0\right)\cos(\omega_0\tau_0) + \left(-3c_1\omega_0^2 + c_3 - c_{10}\right)\sin(\omega_0\tau_0) + 2c_6\omega_0 \\ n_3 = \left(-c_{10}\omega_0^2 - c_1\omega_0^4 + c_3\omega_0^2\right)\cos(\omega_0\tau_0) + \left(-c_9\omega_0^3 + \omega_0^5 + c_{11}\omega_0 - c_2\omega_0^3 + c_4\omega_0\right)\sin(\omega_0\tau_0) \\ n_4 = \left(-c_9\omega_0^3 - \omega_0^5 + c_{11}\omega_0 + c_2\omega_0^3 - c_4\omega_0\right)\cos(\omega_0\tau_0) + \left(c_{10}\omega_0^2 - c_1\omega_0^4 + c_3\omega_0^2\right)\sin(\omega_0\tau_0) \end{cases}. \tag{16}$$

Proof. To establish Hopf bifurcation at $\tau = \tau_0$, we need to verify that $\frac{d(\mathrm{Re}\,\lambda)}{d\tau}\Big|_{\tau=\tau_0} \neq 0$. Notice that $\mathrm{sign}\left[\frac{d(\mathrm{Re}\,\lambda)}{d\tau}\Big|_{\tau=\tau_0}\right] = \mathrm{sign}\left[\mathrm{Re}\left(\frac{\mathrm{d}\lambda}{\mathrm{d}\tau}\right)^{-1}\Big|_{\tau=\tau_0}\right]$ (Feng et al., 2012), then we only need to show that

$$\mathrm{sign}\left[\mathrm{Re}\left(\frac{\mathrm{d}\lambda}{\mathrm{d}\tau}\right)^{-1}\Big|_{\tau=\tau_0}\right] \neq 0.$$

Differentiating Eq. (12) implicitly with respect to τ, we have

$$\begin{aligned} &\left[\left(4\lambda^3 + 3c_1\lambda^2 + 2c_2\lambda + c_3\right)e^{\lambda\tau} + \left(\lambda^4 + c_1\lambda^3 + c_2\lambda^2 + c_3\lambda + c_4\right)\tau e^{\lambda\tau}\right. \\ &\left. + \left(3c_5\lambda^2 + 2c_6\lambda + c_7\right) + \left(2c_9\lambda + c_{10} - c_9\lambda^2\tau - c_{10}\lambda\tau - c_{11}\tau\right)e^{-\lambda\tau}\right]\frac{\mathrm{d}\lambda}{\mathrm{d}\tau} \\ &= \left(c_9\lambda^3 + c_{10}\lambda^2 + c_{11}\lambda\right)e^{-\lambda\tau} - \left(\lambda^5 + c_1\lambda^4 + c_2\lambda^3 + c_3\lambda^2 + c_4\lambda\right)e^{\lambda\tau}. \end{aligned}$$

It follows that

$$\frac{d\lambda(\tau)}{d\tau} = \frac{\left(c_9\lambda^3 + c_{10}\lambda^2 + c_{11}\lambda\right)e^{-\lambda\tau} - \left(\lambda^5 + c_1\lambda^4 + c_2\lambda^3 + c_3\lambda^2 + c_4\lambda\right)e^{\lambda\tau}}{\left[\left(4\lambda^3 + 3c_1\lambda^2 + 2c_2\lambda + c_3\right) + \tau\left(\lambda^4 + c_1\lambda^3 + c_2\lambda^2 + c_3\lambda + c_4\right)\right]e^{\lambda\tau} + \left(2c_9\lambda + c_{10} - c_9\lambda^2\tau - c_{10}\lambda\tau - c_{11}\right)e^{-\lambda\tau} + \left(3c_5\lambda^2 + 2c_6\lambda + c_7\right)}.$$

Combining Eq. (11), then we can get

$$\left(\frac{d\lambda(\tau)}{d\tau}\right)^{-1} = \frac{\left(4\lambda^3 + 3c_1\lambda^2 + 2c_2\lambda + c_3\right)e^{\lambda\tau} + \left(2c_9\lambda + c_{10}\right)e^{-\lambda\tau} + 3c_5\lambda^2 + 2c_6\lambda + c_7}{\left(c_9\lambda^3 + c_{10}\lambda^2 + c_{11}\lambda\right)e^{-\lambda\tau} - \left(\lambda^5 + c_1\lambda^4 + c_2\lambda^3 + c_3\lambda^2 + c_4\lambda\right)e^{\lambda\tau}} - \frac{\tau}{\lambda}. \tag{17}$$

Letting $\tau = \tau_0$, and substituting $\lambda = iw_0$ into Eq. (17), one follows that

$$\left(\frac{d\lambda(\tau)}{d\tau}\right)^{-1}\Big|_{\tau=\tau_0} = \frac{n_1 + in_2}{n_3 + in_4} - \frac{\tau}{\lambda},$$

where $k_i (i = 1, 2, 3, 4)$ are defined in Eq. (16). Therefore,

$$\mathrm{Re}\left[\left(\frac{\mathrm{d}\lambda}{\mathrm{d}\tau}\right)^{-1}\Big|_{\tau=\tau_0}\right] = \frac{n_1 n_3 + n_2 n_4}{n_3^2 + n_4^2} \neq 0.$$

Consequently, according to the Hopf bifurcation theory (Hassard et al., 1981), Hopf bifurcation occurs at E_1 in the system (9) when $\tau = \tau_0$.

4.2. Hybrid bifurcation control strategy of malware propagation in CPSs

According to Theorem 5, the occurrence of Hopf bifurcation takes place when $\tau = \tau_0$, resulting in the instability of system in Eq. (9). In order to effectively control the system, we employ a new hybrid control strategy that integrates parameter adjustment and a memory feedback controller to utilize the time delay.

The hybrid bifurcation control strategy is designed as follows,

$$u(t) = (k_1 - 1)(\beta_1\widetilde{I}_1(t) + \beta_2\widetilde{I}_2(t) - d\widetilde{Q}(t) - r\widetilde{Q}(t-\tau)) + k_2\widetilde{Q}(t-\tau), \tag{18}$$

where k_1 and k_2 are the parameters of the control method.

Remark 2. For the bifurcation caused by the malware in CPSs, various control strategies (Kumari and Upadhyay, 2021; Zhu et al., 2019; Dong and Zhao, 2022; Tian et al., 2023; Yang et al., 2023) are proposed to extend the stable region of the system and delay the shocks and chaos of Hopf bifurcation. However, these articles do not consider utilizing the system's time delay to enhance the stability of the system. Based on this consideration, the system's time delay is incorporated, which effectively delays the Hopf bifurcation and provides better control. Moreover, two adjustment parameters, k_1, k_2, are introduced in Eq. (18), making the control strategy more flexible.

Since Q nodes act as quarantine nodes to isolate the two kinds of infected nodes I_1 and I_2 to prevent the infection from spreading further, controlling the state of Q nodes is crucial for suppressing infection transmission and maintaining the stability of the system. Therefore, we apply

hybrid control to the $\frac{d\widetilde{Q}(t)}{dt}$ in Eq. (9), and the following control system can be obtained,

$$\begin{cases} \frac{d\widetilde{I_1}(t)}{dt} = [\alpha_1(1-\widetilde{I_1}(t)-\widetilde{I_2}(t)-\widetilde{Q}(t)-\widetilde{R}(t))-\beta_1-d-a]\widetilde{I_1}(t) \\ \frac{d\widetilde{I_2}(t)}{dt} = [\alpha_2(1-\widetilde{I_1}(t)-\widetilde{I_2}(t)-\widetilde{Q}(t)-\widetilde{R}(t))-\beta_2-d-b]\widetilde{I_2}(t) \\ \frac{d\widetilde{Q}(t)}{dt} = k_1(\beta_1\widetilde{I_1}(t)+\beta_2\widetilde{I_2}(t)-d\widetilde{Q}(t))+(k_2-rk_1)\widetilde{Q}(t-\tau) \\ \frac{d\widetilde{R}(t)}{dt} = r\widetilde{Q}(t-\tau)+a\widetilde{I_1}(t)+b\widetilde{I_2}(t)-s\widetilde{R}(t-\tau)-d\widetilde{R}(t) \end{cases}. \tag{19}$$

Theorem 6. *Consider system (19) with the hybrid control method in Eq. (18), the threshold value τ_0 can be changed by adjusting the control parameters k_1 and k_2, delaying the occurrence of the Hopf bifurcation.*

Proof. The controlled system (19) shares the same R_0 as the uncontrolled system (9). When $R_0 > 1$ and $R_1 > R_2$, system (19) has one endemic equilibrium point $E_3 = (I_{1h}, I_{2h}, Q_h, R_h)$, where

$$I_{1h} = \frac{d(d+s)(1-S_h)(dk_1-k_2+k_1r)}{\alpha_1 S_h d[k_1(d+r)-k_2]+s(\beta_1+d)(k_1d-k_2)+k_1rds}, \quad I_{2h} = 0,$$
$$Q_h = \frac{k_1d\beta_1(d+s)(1-S_h)}{\alpha_1 S_h d[k_1(d+r)-k_2]+s(\beta_1+d)(k_1d-k_2)+k_1rds}, \quad R_h = \frac{d(1-S_h)[k_1(ad+ar+\beta_1r)-ak_2]}{\alpha_1 S_h d[k_1(d+r)-k_2]+s(\beta_1+d)(k_1d-k_2)+k_1rds}.$$

After simple calculation, we can obtain $S_h = \frac{a+\beta_1+d}{\alpha_1}$. Similar to the previous analysis, we obtain the characteristic equation at E_3 of the controlled system in Eq. (19),

$$0 = \det\begin{bmatrix} \lambda+\alpha_1 I_{1h} & \alpha_1 I_{1h} & \alpha_1 I_{1h} & \alpha_1 I_{1h} \\ 0 & \lambda+\beta_2+d+b-\alpha_2 S_h & 0 & 0 \\ -k_1\beta_1 & -k_1\beta_2 & \lambda+k_1d+(rk_1-k_2)e^{-\lambda\tau} & 0 \\ -a & -b & -re^{-\lambda\tau} & \lambda+d+se^{-\lambda\tau} \end{bmatrix}, \tag{20}$$

namely,

$$\lambda^4+c_{d1}\lambda^3+c_{d2}\lambda^2+c_{d3}\lambda+c_{d4}+(c_{d5}\lambda^3+c_{d6}\lambda^2+c_{d7}\lambda+c_{d8})e^{-\lambda\tau}+(c_{d9}\lambda^2+c_{d10}\lambda+c_{d11})e^{-2\lambda\tau}=0, \tag{21}$$

where

$$\begin{aligned}
c_{d1} &= b+\beta_2+2d+I_{1h}\alpha_1-S_h\alpha_2+dk_1, \\
c_{d2} &= bd+\beta_2 d+2d^2k_1+d^2+I_{1h}a\alpha_1+I_{1h}\alpha_1 b+I_{1h}\alpha_1\beta_2+2I_{1h}\alpha_1 d-S_h\alpha_2 d+bdk_1+\beta_2 dk_1-I_{1h}S_h\alpha_1\alpha_2 \\
&\quad +I_{1h}\alpha_1\beta_1k_1+I_{1h}\alpha_1 dk_1-S_h\alpha_2 dk_1, \\
c_{d3} &= d^3k_1+I_{1h}\alpha_1 d^2+bd^2k_1+\beta_2 d^2k_1+2I_{1h}\alpha_1 d^2k_1-S_h\alpha_2 d^2k_1+I_{1h}a\alpha_1 b+I_{1h}a\alpha_1\beta_2+I_{1h}a\alpha_1 d+I_{1h}\alpha_1 bd \\
&\quad +I_{1h}\alpha_1\beta_2 d-I_{1h}S_h a\alpha_1\alpha_2-I_{1h}S_h\alpha_1\alpha_2 d+I_{1h}\alpha_1 b\beta_1k_1+I_{1h}\alpha_1\beta_1\beta_2k_1+I_{1h}a\alpha_1 dk_1+I_{1h}\alpha_1 bdk_1+2I_{1h}\alpha_1 \\
&\quad \beta_1 dk_1+I_{1h}\alpha_1\beta_2 dk_1-I_{1h}S_h\alpha_1\alpha_2\beta_1k_1-I_{1h}S_h\alpha_1\alpha_2 dk_1, \\
c_{d4} &= I_{1h}\alpha_1 d^3k_1+I_{1h}a\alpha_1 d^2k_1+I_{1h}\alpha_1 bd^2k_1+I_{1h}\alpha_1\beta_1 d^2k_1+I_{1h}\alpha_1\beta_2 d^2k_1+I_{1h}a\alpha_1 bdk_1+I_{1h}a\alpha_1\beta_2 dk_1+I_{1h}\alpha_1 \\
&\quad b\beta_1 dk_1+I_{1h}\alpha_1\beta_1\beta_2 dk_1-I_{1h}S_h\alpha_1\alpha_2 d^2k_1-I_{1h}S_h a\alpha_1\alpha_2 dk_1-I_{1h}S_h\alpha_1\alpha_2\beta_1 dk_1, \quad c_{d5} = -k_2+s+k_1r, \\
c_{d6} &= -bk_2-\beta_2k_2-2dk_2+bs+\beta_2 s+ds-I_{1h}\alpha_1k_2+I_{1h}\alpha_1 s+S_h\alpha_2k_2-S_h\alpha_2 s+bk_1r+\beta_2k_1r+2dk_1r+dk_1s \\
&\quad +I_{1h}\alpha_1k_1r-S_h\alpha_2k_1r, \\
c_{d7} &= -d^2k_2-bdk_2-\beta_2 dk_2-I_{1h}a\alpha_1k_2-I_{1h}\alpha_1 bk_2-I_{1h}\alpha_1\beta_2k_2-2I_{1h}\alpha_1 dk_2+I_{1h}\alpha_1 bs+I_{1h}\alpha_1\beta_2 s+I_{1h}\alpha_1 ds \\
&\quad +S_h\alpha_2 dk_2+bdk_1r+\beta_2 dk_1r+bdk_1s+\beta_2 dk_1s+I_{1h}S_h\alpha_1\alpha_2k_2-I_{1h}S_h\alpha_1\alpha_2 s+I_{1h}a\alpha_1k_1r+I_{1h}\alpha_1 bk_1r+I_{1h} \\
&\quad \alpha_1\beta_1k_1r+I_{1h}\alpha_1\beta_2k_1r+I_{1h}\alpha_1\beta_1k_1s+2I_{1h}\alpha_1 dk_1r+I_{1h}\alpha_1 dk_1s-S_h\alpha_2 dk_1r-S_h\alpha_2 dk_1s-I_{1h}S_h\alpha_1\alpha_2k_1r, \\
c_{d8} &= -I_{1h}\alpha_1 d^2k_2+I_{1h}\alpha_1 d^2k_1r+I_{1h}\alpha_1 d^2k_1s-I_{1h}a\alpha_1 bk_2-I_{1h}a\alpha_1\beta_2k_2-I_{1h}a\alpha_1 dk_2-I_{1h}\alpha_1 bdk_2-I_{1h}\alpha_1\beta_2 dk_2 \\
&\quad +I_{1h}S_h a\alpha_1\alpha_2k_2+I_{1h}S_h\alpha_1\alpha_2 dk_2+I_{1h}a\alpha_1 bk_1r+I_{1h}a\alpha_1\beta_2k_1r+I_{1h}\alpha_1 b\beta_1k_1r+I_{1h}\alpha_1\beta_1\beta_2k_1r+I_{1h}a\alpha_1 dk_1r \\
&\quad +I_{1h}\alpha_1 b\beta_1k_1s+I_{1h}\alpha_1\beta_1\beta_2k_1s+I_{1h}\alpha_1 bdk_1r+I_{1h}\alpha_1\beta_1 dk_1r+I_{1h}\alpha_1\beta_2 dk_1r+I_{1h}\alpha_1 bdk_1s+I_{1h}\alpha_1\beta_1 dk_1s \\
&\quad +I_{1h}\alpha_1\beta_2 dk_1s-I_{1h}S_h a\alpha_1\alpha_2k_1r-I_{1h}S_h\alpha_1\alpha_2\beta_1k_1r-I_{1h}S_h\alpha_1\alpha_2\beta_1k_1s-I_{1h}S_h\alpha_1\alpha_2 dk_1r-I_{1h}S_h\alpha_1\alpha_2 dk_1s, \\
c_{d9} &= -k_2s+k_1rs+d^2k_1r+d^2k_1s, \\
c_{d10} &= -bk_2s-\beta_2k_2s-dk_2s-I_{1h}\alpha_1k_2s+S_h\alpha_2k_2s+bk_1rs+\beta_2k_1rs+dk_1rs-S_h\alpha_2k_1rs+I_{1h}\alpha_1k_1rs, \\
c_{d11} &= -I_{1h}\alpha_1\beta_2k_2s-I_{1h}\alpha_1 dk_2s+I_{1h}S_h\alpha_1\alpha_2k_2s+I_{1h}\alpha_1 bk_1rs+I_{1h}\alpha_1\beta_2k_1rs+I_{1h}\alpha_1 dk_1rs-I_{1h}S_h\alpha_1\alpha_2k_1rs.
\end{aligned}$$

Similar to the proof of Hopf bifurcation analysis in Section 4.1, the Hopf bifurcation threshold τ_0 and the corresponding ω_0 of the controlled system (19) can be calculated. By adjusting the parameters k_1 and k_2, the value of τ_0 can be changed, reducing the harm caused by malware propagating in CPSs.

5. Numerical simulation and analysis

To illustrate the validity and merits of the theoretical analysis, in this section, two parts of the numerical simulation are provided.

5.1. Dynamic behavior simulations

We conduct numerical simulations to analyze the dynamic behavior of the proposed SI2QRS model and validate the effectiveness of the hybrid control method.

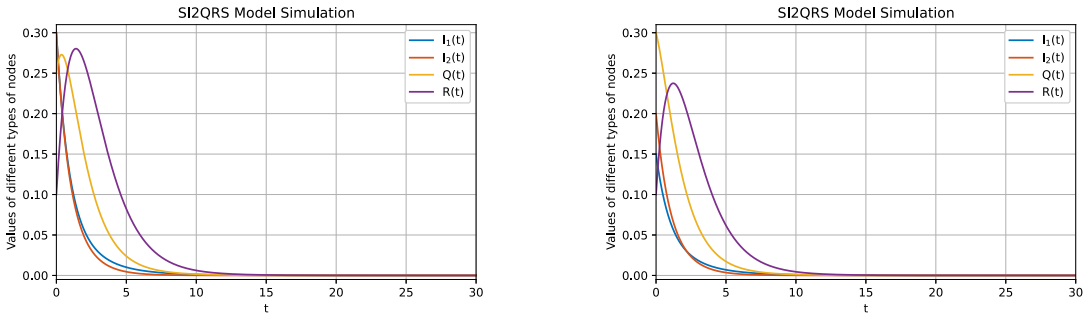

(a) Evolution curves with initial values $(0.3, 0.3, 0.25, 0.1)$. (b) Evolution curves with initial values $(0.15, 0.2, 0.3, 0.1)$.

Fig. 3. Evolution curves of I_1, I_2, Q and R when $R_0 < 1$ with different initial values.

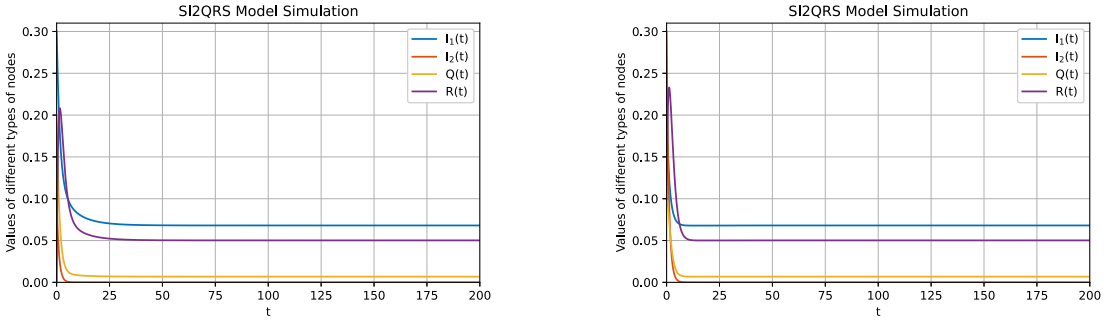

(a) Evolution curves with initial values $(0.3, 0.1, 0.2, 0)$. (b) Evolution curves with initial values $(0.2, 0.3, 0.1, 0.1)$.

Fig. 4. Evolution curves of I_1, I_2, Q and R when $R_0 > 1$ and $R_1 > R_2$ with different initial values.

5.1.1. Dynamic behavior simulation of SI2QRS

We verify the stability of the SI2QRS model in Eq. (2) under different cases through simulations. We set the initial densities of all kinds of nodes in CPSs with two different sets of values: $(I_1(0), I_2(0), Q(0), R(0)) = (0.3, 0.3, 0.25, 0.1)$ and $(I_1(0), I_2(0), Q(0), R(0)) = (0.15, 0.2, 0.3, 0.1)$, respectively. Moreover, the chosen parameter values are as follows: $\alpha_1 = 0.6, \alpha_2 = 0.3, \beta_1 = 0.6, \beta_2 = 0.7, d = 0.1, a = 0.3, b = 0.2, s = 0.7$ and $r = 0.9$. By calculating, the basic reproductive number $R_0 = 0.6 < 1$, which satisfies the conditions of Theorem 1. Therefore, there is only one disease-free equilibrium point E_0. The trajectories of the system (2) at E_0 with two different initial values are shown in Fig. 3. From Fig. 3, it can be observed that the system is asymptotically stable at E_0 when $R_0 < 1$, which is consistent with Theorem 1.

Now, we validate Theorem 2. By setting $\alpha_1 = 0.8, \alpha_2 = 0.1, \beta_1 = 0.1, \beta_2 = 0.3, d = 0.1, a = 0.5, b = 0.6, s = 0.7,$ and $r = 0.9$, we can determine that $R_0 = 1.1429 > 1$ and $R_1 > R_2$. Using the initial values as $(0.3, 0.1, 0.2, 0), (0.2, 0.3, 0.1, 0.1)$, one can obtain $E_1 = (0.0680, 0, 0.0068, 0.0502)$. Fig. 4 shows the trajectories of the four given types of nodes in the system at E_1, which indicates the asymptotic stability of system at E_1, thereby confirming the assertion of Theorem 2.

Similarly, we verify Theorem 3. By setting $\alpha_1 = 0.6, \alpha_2 = 0.8, \beta_1 = 0.2, \beta_2 = 0.1, d = 0.1, a = 0.2, b = 0.4, s = 0.7,$ and $r = 0.9$, it can be obtained that $R_0 = 1.33 > 1$ and $R_2 > R_1$. By calculation, $E_2 = (0, 0.1460, 0.0146, 0.0894)$. Setting initial values as $(0.5, 0.1, 0.2, 0.1)$ and $(0.3, 0.3, 0.1, 0.1)$, from Fig. 5, the trajectories of $I_1(t)$ converges to 0, $I_2(t)$ converges to 0.146, $Q(t)$ converges to 0.0146, $R(t)$ converges to 0.0894. It indicates the asymptotic stability of system (2) at E_2, thereby confirming the assertion of Theorem 3.

5.1.2. Dynamic behavior simulation of SI2QRS with time delay

To verify Theorem 4, By setting $\alpha_1 = 0.8, \alpha_2 = 0.3, \beta_1 = 0.1, \beta_2 = 0.3, d = 0.1, a = 0.5, b = 0.6, s = 0.7,$ and $r = 0.9$, we can determine that $R_0 = 1.1429 > 1$ and $R_1 > R_2$, and choose the initial value as $(I_1, I_2, Q, R) = (0.1, 0.1, 0.1, 0.2)$. Considering the model (9), by referring Eq. (14) and (15), it is obtained that $\tau_0 = 1.9433$. In order to verify the conclusion in Theorem 4, let $\tau = 1.7 < \tau_0$, Fig. 6(a) shows that the system is locally asymptotically stable at $E_1 = (0.0680, 0, 0.0068, 0.0502)$, which confirms the assertion of Theorem 4. To verify Theorem 5, We now choose $\tau = 1.941$, which is very close to τ_0, and Fig. 6(b) shows that E_1 progressively loses stability, resulting in the occurrence of Hopf bifurcation. Therefore, the above simulation result verifies Theorem 5.

5.1.3. Hybrid bifurcation control simulation

In this subsection, we validate the hybrid bifurcation control strategy for Hopf bifurcation. Letting $\alpha_1 = 0.8, \alpha_2 = 0.3, \beta_1 = 0.1, \beta_2 = 0.3, d = 0.1, a = 0.5, b = 0.6, s = 0.7,$ and $r = 0.9$, we can determine that $R_0 = 1.1429 > 1$ and $R_1 > R_2$. As shown in Fig. 6(b), Hopf bifurcation occurs when $\tau = 1.941$. Then under the controller (18) with $k_1 = 0.9$ and $k_2 = 0.3$, the trajectories of system (2) is shown in Fig. 7, one finds it gradually converge to $E_1 = (0.0680, 0, 0.0068, 0.0502)$. Therefore, the Hopf bifurcation can be controlled by the proposed hybrid approach.

When $\tau = 1.98$, the uncontrolled system (9) in Fig. 8(a) is unstable, while the trajectories of the system (19) under the controller (18) with $k_1 = 0.9$ and $k_2 = 0.3$ gradually converge to E_1, as shown in Fig. 8(b). Thus, it can be obtained that the control method can delay the occurrence of the Hopf bifurcation and provides better control.

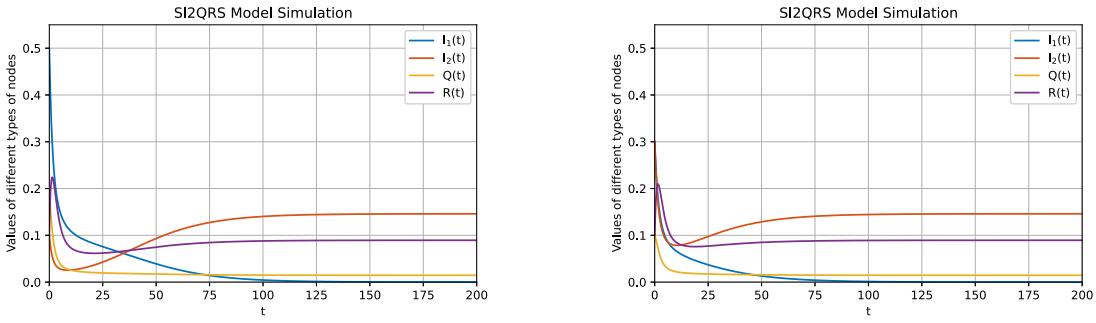

(a) Evolution curves with initial values $(0.5, 0.1, 0.2, 0.1)$. (b) Evolution curves with initial values $(0.3, 0.3, 0.1, 0.1)$.

Fig. 5. Evolution curves of I_1, I_2, Q and R when $R_0 > 1$ and $R_2 > R_1$ with different initial values.

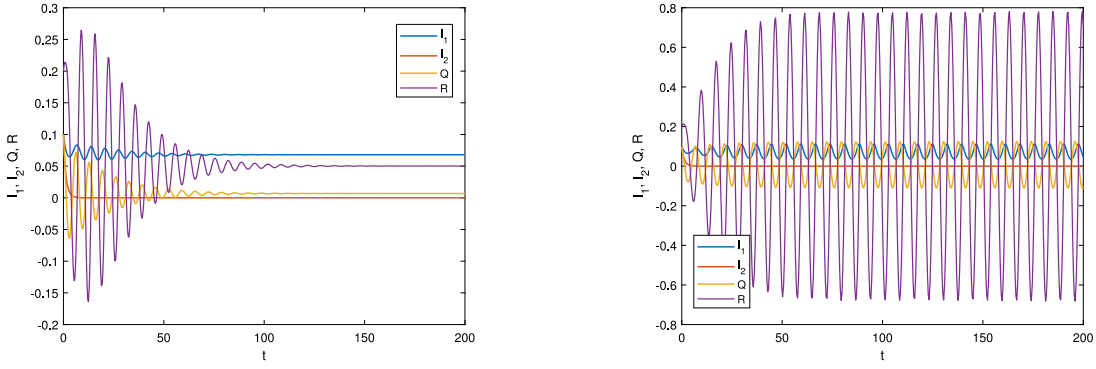

(a) Evolution curves when $\tau = 1.7$. (b) Evolution curves when $\tau = 1.941$.

Fig. 6. Evolution curves of I_1, I_2, Q and R.

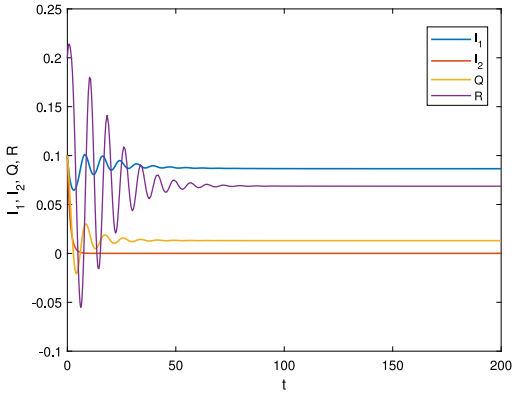

Fig. 7. System trajectories under the controller (18) with $k_1 = 0.9$ and $k_2 = 0.3$ when $\tau = 1.941$.

Table 2
τ_0 and ω_0 corresponding to the different k_1 and k_2.

k_1	k_2	τ_0	ω_0
1	0	1.9433	0.8780
0.9	0	2.2000	0.8048
0.9	0.3	2.3529	0.7597
0.7	0.5	2.9580	0.3858

Now, we demonstrate the flexibility of the parameters adjusting the Hopf bifurcation threshold. By changing the value of the parameters k_1 and k_2, the corresponding ω_0 and τ_0 can be calculated, as shown in Table 2. Considering k_1 and k_2 as independent variables, τ_0 as dependent variable, we set the step size to 0.1 and plot $\tau_0(k_1, k_2)$ on the interval $[0, 5]$, as shown in Fig. 9. From Table 2 and Fig. 9, it can be obtained that the threshold of the system can be increased by changing the value of two parameters, thereby validating Theorem 6.

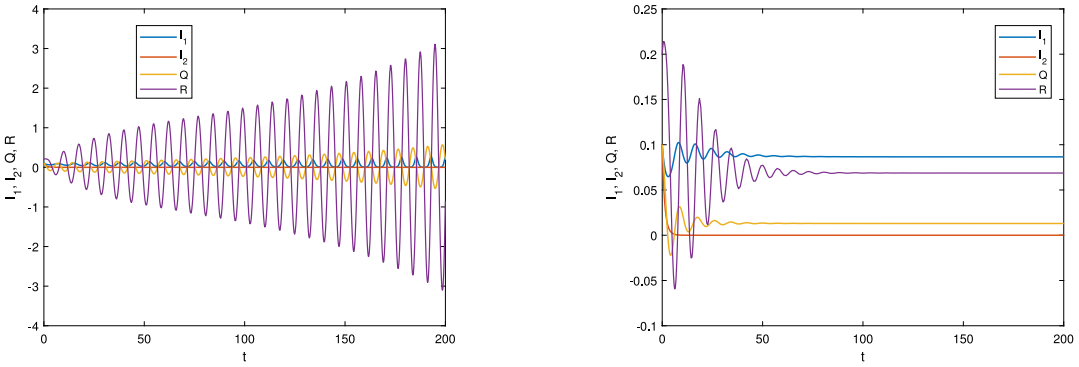

(a) Evolution curves when $\tau = 1.98$. (b) Controlled system when $\tau = 1.98$.

Fig. 8. Evolution curves of I_1, I_2, Q and R.

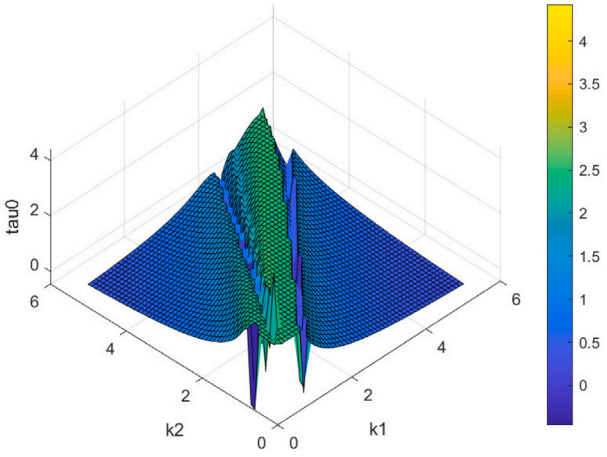

Fig. 9. The approximative curve of $\tau_0(k_1, k_2)$.

5.2. Experimental analysis

Based on Theorem 1, this example is given to show the real application of the SI2QRS model. By the real dataset of networks of computing hosts[1] provided by the Stanford Network Analysis Platform at Stanford University, we use the Mirai propagation to validate the model in CPSs. From the dataset, we consider 56 047 nodes and 56 773 edges of the computing hosts. And the Mirai propagation process is shown in Fig. 10.

As illustrated in Fig. 10, in the first stage of Mirai's propagation, the attacker remotely scans and attacks CPS devices via Telnet or SSH, exploiting weak passwords to successfully infect the devices. After infection, the devices download and execute the malware, becoming the initial infected devices. These infected devices then wait for instructions from the C&C server. Upon receiving a propagation command, they begin to randomly attack other devices. Mirai may initially behave as a typical worm virus during its early stages, but as the worm evolves and upgrades itself throughout the propagation process, its infectivity and malicious behavior can be significantly enhanced. This characteristic allows Mirai to bypass conventional security defenses, rapidly expanding and infecting a broader range of devices.

Based on the above description, the process is described by:

$$\begin{cases} \frac{dS(t)}{dt} = d(N - S(t)) - \frac{\alpha_1 S(t) I_1(t)}{N} - \frac{\alpha_2 S(t) I_2(t)}{N} + sR(t) \\ \frac{dI_1(t)}{dt} = \frac{\alpha_1 S(t) I_1(t)}{N} - \beta_1 I_1(t) - d I_1(t) - a I_1(t) \\ \frac{dI_2(t)}{dt} = \frac{\alpha_2 S(t) I_2(t)}{N} - \beta_2 I_2(t) - d I_2(t) - b I_2(t) \\ \frac{dQ(t)}{dt} = \beta_1 I_1(t) + \beta_2 I_2(t) - rQ(t) - dQ(t) \\ \frac{dR(t)}{dt} = rQ(t) + a I_1(t) + b I_2(t) - sR(t) - d R(t) \end{cases}, \tag{22}$$

where $S(t), I_1(t), I_2(t), Q(t), R(t) \geq 0$.

There is a more detailed explanation of the node types of the Mirai propagation process in CPSs:

1. Susceptible Nodes S: Initially, all devices with security vulnerabilities belong to the susceptible node category. These devices have not yet been infected, but due to the lack of protective mechanisms, they are highly vulnerable to attack.

[1] https://snap.stanford.edu/data/cisco-networks.

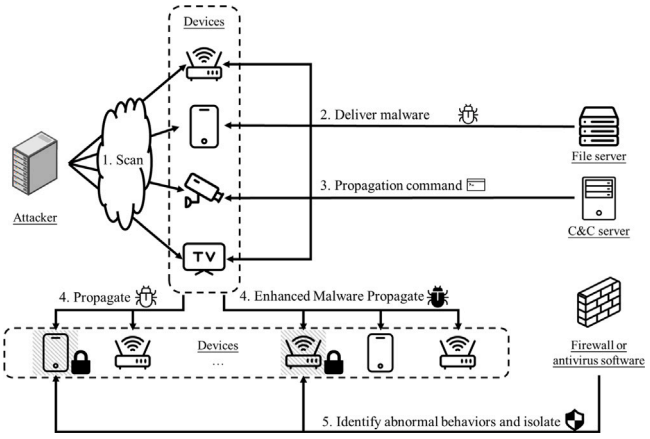

Fig. 10. Mirai propagation process in CPSs.

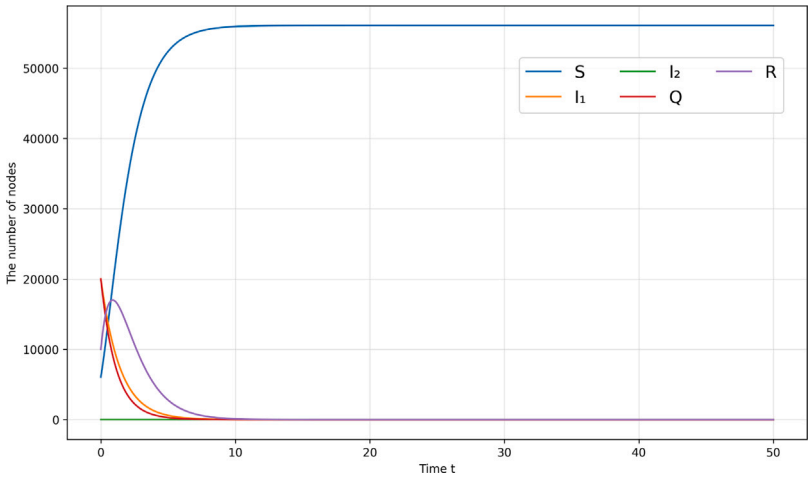

Fig. 11. Trajectories of S, I_1, I_2, Q and R by simulation.

2. Infected Nodes I_1: The attacker uses Telnet or SSH to brute-force attack devices on the network. Once successful, the malicious software is transferred to the target device, which then becomes an initial infected node I_1. In this state, the device has been infected and begins to wait for further instructions from the command and control (C&C) server.

3. Enhanced Infected Nodes I_2: As Mirai propagates, it may self-update to enhance its propagation capabilities, tailored to the CPS environment. Some infected devices transform into Enhanced Infected Nodes $I_2(t)$, which have a higher propagation capability and may adopt different strategies to bypass defense systems.

4. Quarantine Nodes Q: As security defense systems (such as firewall or antivirus software) detect abnormal traffic or behavior, propagating devices may be isolated. For example, a system administrator might disconnect infected devices from the network or block their communication ports. In this case, the devices enter quarantine state Q, no longer participating in propagation.

5. Recovered Nodes R: Infected or quarantined devices that have undergone antivirus scanning, system updates, or security hardening can recover and return to normal operation, entering recovery state R. Devices in this state are temporarily immune and will not be infected again unless their immunity is compromised.

6. Immunity Failure and Reversion to S: Over time, some recovered nodes may fail to maintain adequate security measures, leading to weakened or lost immunity. These devices will revert back to susceptible nodes S, re-entering the infection cycle.

To validate the SI2QRS model, we set the parameters as $\alpha_1 = 0.0008, \alpha_2 = 0.0001, \beta_1 = 0.1, \beta_2 = 0.3, d = 0.1, a = 0.5, b = 0.6, s = 0.7,$ and $r = 0.9$, we let $R_0 < 1$. And the initial values of the nodes are $[S, I_1, I_2, Q, R] = [6047, 20\,000, 0, 20\,000, 10\,000]$. And the trajectories of S, I_1, I_2, Q and R can be obtained, shown in Fig. 11. From Fig. 11, it can be observed that the system reaches a stable state at (56 047,0,0,0,0) when $R_0 < 1$, which is consistent with Theorem 1.

To further validate the effectiveness of the model on the real dataset, based on the algorithm in Zhu et al. (2023), an algorithm is expanded, shown in Algorithm 1. We denote the results obtained from the algorithm as $S_r, I_{1r}, I_{2r}, Q_r, R_r$, the result is shown in Fig. 12. Compared Fig. 11

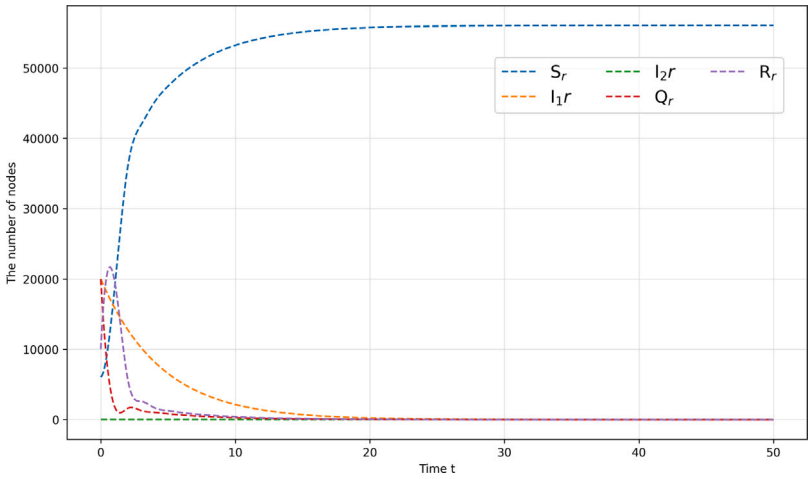

Fig. 12. Trajectories of S, I_1, I_2, Q and R by Algorithm 1.

with Fig. 12, it can be observed that both results exhibit similar trends across all states, and the trajectories by the differential equation method converges earlier than that obtained by Algorithm 1.

Algorithm 1: The spread of Mirai in CPSs.

Input: Initialize the network $G = (v, e)$ with the given data set and randomly assign the initial number of nodes in each state.
Output: The number of S, I_1, I_2, Q, and R nodes at time t^*
for $t = 0$ ***to*** t^* ***with the step of*** Δt **do**
  if *node(i) in the state S and do not leave the network* **then**
    if *affected by infected nodes* **then**
      it will become I_1 (or I_2) with probability α_1 (or α_2);
    end
    else
      its state remains unchanged;
    end
  end
  else if *node(i) in the state* I_1 *(or* I_2*) and do not leave the network* **then**
    if *the malware gets quarantined after firewalls identify abnormal behaviors* **then**
      it will become Q with probability β_1 (or β_2);
    end
    else if *the malware is detected and removed by the anti-virus software* **then**
      it will become R with probability a (or b);
    end
    else
      its state remains unchanged;
    end
  end
  else if *node(i) in the state R and do not leave the network* **then**
    if *recovered devices lose immunity* **then**
      it will become S with probability s;
    end
    else
      its state remains unchanged;
    end
  end
end

6. Conclusions

In this paper, we investigate the modeling and hybrid control of malware propagation in CPSs. Considering that malware may enhance its infection capability during propagation, we propose a malware model with two distinct infection rates and analyze its dynamic behavior. Given the inevitability of time delays in CPSs, we introduce a time delay into the SI2QRS model. Since time delays may induce bifurcation, we derive the conditions for bifurcation occurrence and design a hybrid control strategy with adjustable parameters. Theoretical analysis and simulation results demonstrate that the proposed control method can effectively suppress malware propagation and maintain the stable operation of the system. In practical CPSs applications, computing and network resources are often limited, necessitating more efficient control mechanisms. In future work, optimal control strategies, which integrate the reinforcement learning (RL) with model predictive control (MPC) (Jafar et al., 2024, 2025), will be designed to save the limited communication resources for CPSs.

CRediT authorship contribution statement

Huifang Xiang: Writing – original draft, Visualization, Validation, Methodology, Investigation, Conceptualization. **Ruimei Zhang:** Writing – review & editing, Supervision, Conceptualization. **Ziling Wang:** Visualization. **Di Dong:** Writing – review & editing.

Declaration of competing interest

The authors declare that they have no known competing financial interests or personal relationships that could have appeared to influence the work reported in this paper.

Acknowledgments

The work was supported by the National Natural Science Foundation of China under Grant 62376171 and the Program of Science and Technology of Sichuan Province of China under Grant 2023NSFSC0477.

Appendix A. The proof of $\Delta_1 > 0$, $\Delta_2 > 0$ and $\Delta_3 > 0$ in Theorem 2

Proof. Consider the characteristic polynomial of J_{E_1} when $R_0 > 1, R_1 > R_2$:

$$\lambda^4 + a_1\lambda^3 + a_2\lambda^2 + a_3\lambda + a_4 = 0,$$

where

$$a_1 = q_1 + q_2, \quad a_2 = q_1q_2 + q_3, \quad a_3 = q_1q_3 + q_4, \quad a_4 = q_1q_4,$$

and

$$\begin{aligned}
q_1 &= b + \beta_2 + d - \alpha_2 S^*,\\
q_2 &= 2d + r + s + \alpha_1 I_1^*,\\
q_3 &= dr + ds + rs + d^2 + \alpha_1 I_1^*(a + \beta_1 + 2d + r + s),\\
q_4 &= \alpha_1 I_1^*(d^2 + ad + \beta_1 d + ar + \beta_1 r + \beta_1 s + dr + ds + rs).
\end{aligned}$$

Since $R_0 = R_1 > 1 > R_2$, it follows that $S^* < 1 < S_e$. Since $S_e = \frac{b+\beta_2+d}{\alpha_2}$, it is clear that $\alpha_2 S_e = b + \beta_2 + d$, thus $\alpha_2 S^* < b + \beta_2 + d$, which implies that $q_1 = b + \beta_2 + d - \alpha_2 S^* > 0$. Also, it is evident that $q_2, q_3, q_4 > 0$ due to all parameters being positive. So we can obtain that $a_1, a_2, a_3, a_4 > 0$.

Then, we obtain

$$\begin{aligned}
\Delta_1 &= a_1 = q_1 + q_2 > 0,\\
\Delta_2 &= a_1a_2 - a_3 = (q_1 + q_2)(q_2 + q_3) - q_1q_3 - q_4,\\
\Delta_3 &= a_1\left(a_2a_3 - a_1a_4\right) - a_3^2 = (q_1 + q_2)(q_2 + q_3)q_1q_3 - (q_1 + q_2)^2q_1q_4 - (q_1q_3)^2.
\end{aligned}$$

The Routh–Hurwitz stability criterion requires that the above parameters are positive. As can be seen from the above, $\Delta_1 > 0$. Next, we will prove that $\Delta_2, \Delta_3 > 0$. By calculation, we have

$$\begin{aligned}
\Delta_2 &= a_1a_2 - a_3 = (q_1 + q_2)(q_1q_2 + q_3) - (q_1q_3 + q_4),\\
&= q_1^2q_2 + q_1q_3 + q_1q_2^2 + q_2q_3 - q_1q_3 - q_4,\\
&= q_1^2q_2 + q_1q_2^2 + q_2q_3 - q_4.
\end{aligned}$$

Since $q_2q_3 - q_4 > 0$, it is easy to obtain that $\Delta_2 > 0$. Similarly, one has

$$\begin{aligned}
\Delta_3 &= a_1(a_2a_3 - a_1a_4) - a_3^2\\
&= (q_1 + q_2)(q_1q_2 + q_3)(q_1q_3 + q_4) - (q_1 + q_2)^2q_1q_4\\
&= (q_1^2q_2 + q_1q_3 + q_1q_2^2 + q_2q_3)(q_1q_3 + q_4) - (q_1^2 + q_2^2 + 2q_1q_2)q_1q_4\\
&- (q_1^2q_3^2 + q_4^2 + 2q_1q_3q_4)\\
&= (q_1^3q_2q_3 + q_1^2q_2q_4 + q_1^2q_3^2 + q_1q_3q_4 + q_1^2q_2^2q_3 + q_1q_2^2q_4 + q_1q_2q_3^2\\
&+ q_2q_3q_4) - q_1^3q_4 - q_1q_2^2q_4 - 2q_1^2q_2q_4 - q_1^2q_3^2 - q_4^2 - 2q_1q_3q_4\\
&= (q_1^3 + q_1^2q_2 + q_1q_3 + q_4)(q_2q_3 - q_4)
\end{aligned}$$

It is proved that $\Delta_3 > 0$. Therefore, we can prove that $\Delta_1 > 0$, $\Delta_2 > 0$ and $\Delta_3 > 0$.

Appendix B. The stability of the model at E_2 in Theorem 3.

Proof. When $R_0 > 1, R_2 > R_1$, the Jacobian matrix of the system at E_2 is

$$J_{E_2} = \begin{bmatrix}
\alpha_1 S_e - \beta_1 - d - a & 0 & -0 & 0\\
-\alpha_2 I_{2e} & -\alpha_2 I_{2e} & -\alpha_2 I_{2e} & -\alpha_2 I_{2e}\\
\beta_1 & \beta_2 & -d - r & 0\\
a & b & r & -d - s
\end{bmatrix}.$$

The characteristic polynomial of J_{E_2} is $\lambda^4 + a_1\lambda^3 + a_2\lambda^2 + a_3\lambda + a_4 = 0$, where

$$b_1 = l_1 + l_2, \quad b_2 = l_1 l_2 + l_3, \quad b_3 = l_1 l_3 + l_4, \quad b_4 = l_1 l_4,$$

and

$$l_1 = a + \beta_1 + d - S_e\alpha_1, l_3 = dr + ds + rs + d^2 + I_{2e}b\alpha_2 + I_{2e}\alpha_2\beta_2 + 2I_{2e}\alpha_2 d + I_{2e}\alpha_2 r + I_{2e}\alpha_2 s,$$
$$l_2 = 2d + r + s + I_{2e}\alpha_2, l_4 = I_{2e}\alpha_2 d^2 + I_{2e}b\alpha_2 d + I_{2e}\alpha_2\beta_2 d + I_{2e}b\alpha_2 r + I_{2e}\alpha_2\beta_2 r + I_{2e}\alpha_2\beta_2 s + I_{2e}\alpha_2 dr + I_{2e}\alpha_2 ds + I_{2e}\alpha_2 rs.$$

Then, we obtain

$$\Delta_1 = a_1 = l_1 + l_2,$$
$$\Delta_2 = a_1 a_2 - a_3 = (l_1 + l_2)(l_2 + l_3) - l_1 l_3 - l_4,$$
$$\Delta_3 = a_1\left(a_2 a_3 - a_1 a_4\right) - a_3^2 = (l_1 + l_2)(l_2 + l_3) l_1 l_3 - (l_1 + l_2)^2 l_1 l_4 - (l_1 l_3)^2.$$

Data availability

Data will be made available on request.

References

Abidemi, A., Aziz, M.I.A., Ahmad, R., 2020. Mathematical modelling of coexistence of two dengue virus serotypes with seasonality effect. J. Comput. Theor. Nanosci. 17 (2–3), 783–794.

Bailey, N.T.J., 1975. The Mathematical Theory of Infectious Diseases and Its Applications. Charles Griffin & Company Ltd.

Barman, M., Mishra, N., 2024. Hopf bifurcation analysis for a delayed nonlinear-SEIR epidemic model on networks. Chaos Solitons Fractals 178, 114351.

Carnier, R.M., Li, Y., Fujimoto, Y., Shikata, J., 2024. Deriving exact mathematical models of malware based on random propagation. Mathematics 12 (6), 835.

Chen, H., Zong, G., Zhao, X., Gao, F., Shi, K., 2023. Secure filter design of fuzzy switched CPSs with mismatched modes and application: A multidomain event-triggered strategy. IEEE Trans. Ind. Inform. 19 (10), 10034–10044.

Dong, Y., Zhao, L., 2022. An improved two-layer model for rumor propagation considering time delay and event-triggered impulsive control strategy. Chaos Solitons Fractals 164, 112711.

Feng, L., Liao, X., Li, H., Han, Q., 2012. Hopf bifurcation analysis of a delayed viral infection model in computer networks. Math. Comput. Modelling 56 (7–8), 167–179.

Freedman, H.I., Hari Rao, V.S., 1983. The trade-off between mutual interference and time lags in predator-prey systems. Bull. Math. Biol. 45 (6), 991–1004.

Ghousein, M., Moulay, E., Coirault, P., 2023. Semi-Markov models of epidemics over networks with time delays. Internat. J. Robust Nonlinear Control 33 (9), 4761–4783.

Ginters, E., Dumpis, U., Liñán, L.C., Eroles, M.A.P., Nazemi, K., Matvejevs, A., Estrada, M.A.R., 2025. A paradigm for modeling infectious diseases: Assessing malware spread in early-stage outbreaks. Mathematics 13 (1).

Gupta, S., Cherukuri, A.K., Subramanian, C.M., Ahmad, A., 2022. Comparison, analysis and analogy of biological and computer viruses. Intell. Interact. Multimed. Syst. E-Heal. Appl. 3–34.

Hassard, B., Kazarinoff, N.D., Wan, Y.-H., 1981. Theory and Applications of Hopf Bifurcation.

Jafar, M.T., Yang, L., Li, G., 2025. An innovative practical roadmap for optimal control strategies in malware propagation through the integration of RL with MPC. Comput. Secur. 148, 104186.

Jafar, M.T., Yang, L., Li, G.G., Zhu, Q., Gan, C., 2024. Minimizing malware propagation in internet of things networks: An optimal control using feedback loop approach. IEEE Trans. Inf. Forensics Secur. 19, 9682–9697.

Kephart, J.O., White, S.R., 1992. Directed-graph epidemiological models of computer viruses. In: Computation: The Micro and the Macro View. World Scientific, pp. 71–102.

Kermack, W.O., McKendrick, A.G., 1927. A contribution to the mathematical theory of epidemics. Proc. R. Soc. Lond. Ser. A Contain. Pap. A Math. Phys. Character 115 (772), 700–721.

Kharabsheh, M., Al-aiash, I., Mughaid, A., Almiani, M., 2024. The SEIR model for predicting malware propagation in computer networks. In: 2024 International Conference on Intelligent Computing, Communication, Networking and Services. ICCNS, IEEE, pp. 108–113.

Kim, K.S., Ibrahim, M.M., Jung, I.H., Kim, S., 2020. Mathematical analysis of the effectiveness of control strategies to prevent the autorun virus transmission propagation. Appl. Math. Comput. 371, 124955.

Kim, Y.R., Min, Y., Okogun-Odompley, J.N., 2024. A mathematical model of COVID-19 with multiple variants of the virus under optimal control in Ghana. Plos One 19 (7), e0303791.

Kiss, A.K., Molnar, T.G., Ames, A.D., Orosz, G., 2023. Control barrier functionals: Safety-critical control for time delay systems. Internat. J. Robust Nonlinear Control 33 (12), 7282–7309.

Kumari, S., Upadhyay, R.K., 2021. Exploring the dynamics of a malware propagation model and its control strategy. Wirel. Pers. Commun. 121 (3), 1945–1978.

Li, J., Knickerbocker, P., 2007. Functional similarities between computer worms and biological pathogens. Comput. Secur. 26 (4), 338–347.

Li, M.Y., Muldowney, J.S., 2000. Dynamics of differential equations on invariant manifolds. J. Differential Equations 168 (2), 295–320.

Liu, J., Wang, Y., Cao, J., Yue, D., Xie, X., 2021. Secure adaptive-event-triggered filter design with input constraint and hybrid cyber attack. IEEE Trans. Cybern. 51 (8), 4000–4010.

Lu, G., Lu, Z., 2017. Geometric approach to global asymptotic stability for the SEIRS models in epidemiology. Nonlinear Anal. Real World Appl. 36, 20–43.

Lu, G., Lu, Z., 2018. Global asymptotic stability for the SEIRS models with varying total population size. Math. Biosci. 296, 17–25.

Ma, Y.S., Che, W.W., Deng, C., Wu, Z.G., 2023. Distributed model-free adaptive control for learning nonlinear MASs under DoS attacks. IEEE Trans. Neural Netw. Learn. Syst. 34 (3), 1146–1155.

Ma, Y., Tsou, C., 2024. A novel passive-active detection system for false data injection attacks in industrial control systems. Comput. Secur. 145, 103996.

Masood, Z., Samar, R., Raja, M.A.Z., 2019. Design of a mathematical model for the Stuxnet virus in a network of critical control infrastructure. Comput. Secur. 87, 101565.

Namanya, A.P., Cullen, A., Awan, I.U., Disso, J.P., 2018. The world of malware: An overview. In: 2018 IEEE 6th International Conference on Future Internet of Things and Cloud. FiCloud, pp. 420–427.

Oliveira, F., Costa, D.G., Assis, F., Silva, I., 2024. Internet of Intelligent Things: A convergence of embedded systems, edge computing and machine learning. Internet Things 101153.

Signes-Pont, M.T., Cortés-Castillo, A., Mora-Mora, H., Szymanski, J., 2018. Modelling the malware propagation in mobile computer devices. Comput. Secur. 79, 80–93.

Tadmon, C., Fossi, A.F., Tsanou, B., 2024. A two-strain avian–human influenza model with environmental transmission: Stability analysis and optimal control strategies. Commun. Nonlinear Sci. Numer. Simul. 133, 107981.

Tian, L., Shang, F., Gan, C., 2023. Optimal control analysis of malware propagation in cloud environments. Math. Biosci. Eng. 20 (8), 14502–14517.

Van den Driessche, P., Watmough, J., 2002. Reproduction numbers and sub-threshold endemic equilibria for compartmental models of disease transmission. Math. Biosci. 180 (1–2), 29–48.

Wang, Z., Xie, W., Wang, B., Tao, J., Wang, E., 2021. A survey on recent advanced research of CPS security. Appl. Sci. 11 (9), 3751.

Xu, L., Guo, Q., Wang, Z., Sun, H., 2021. Modeling of time-delayed distributed cyber-physical power systems for small-signal stability analysis. IEEE Trans. Smart Grid 12 (4), 3425–3437.

Yang, Y., Liu, G., Liang, Z., Chen, H., Zhu, L., Zhong, X., 2023. Hybrid control for malware propagation in rechargeable WUSN and WASN: From knowledge-driven to data-driven. Chaos Solitons Fractals 173, 113703.

Yang, B., Yu, Z., Cai, Y., 2022. Malicious software spread modeling and control in cyber–physical systems. Knowl.-Based Syst. 248, 108913.

Yu, Z., Gao, H., Cong, X., Wu, N., Song, H., 2023. A survey on cyber-physical systems security. IEEE Internet Things J. 10 (24), 21670–21686.
Zarin, R., Ullah, N., Khan, A., Humphries, U.W., 2023. A numerical study of a new non-linear fractal fractional mathematical model of malicious codes propagation in wireless sensor networks. Comput. Secur. 135, 103484.
Zhang, Y., Pan, D., 2021. Layered SIRS model of information spread in complex networks. Appl. Math. Comput. 411, 126524.
Zhang, H., Upadhyay, R.K., Liu, G., Zhang, Z., 2022. Hopf bifurcation and optimal control of a delayed malware propagation model on mobile wireless sensor networks. Results Phys. 41.
Zhu, L., Guan, G., Li, Y., 2019. Nonlinear dynamical analysis and control strategies of a network-based SIS epidemic model with time delay. Appl. Math. Model. 70, 512–531.
Zhu, Q., Zhang, G., Luo, X., Gan, C., 2023. An industrial virus propagation model based on SCADA system. Inform. Sci. 630, 546–566.